

Rate Meta-Distribution in Millimeter Wave URLLC Device-to-Device Networks with Beam Misalignment

Yibo Quan, Marceau Coupechoux and Jean-Marc Kélif

Abstract—Using the stochastic geometry framework, we study a millimeter wave (mmWave) Device-to-Device (D2D) network dedicated to Ultra-Reliable Low Latency Communications (URLLC), where users employ multiple antennas to perform beamforming. We leverage the notion of meta-distribution in order to capture the reliability requirement of URLLC. The packet transmission process is divided into two phases: a beam training phase, during which exhaustive beam sweeping is adopted, and a data transmission phase. The paper investigates the misalignment error distribution resulting from an imperfect training phase, due to the finite codebooks resolution and the fast variation of the channel. For the data transmission phase, closed-form expressions for all the moments of the conditional rate coverage probability are derived, and the meta-distribution is approximated using the beta approximation. The study evaluates the overall network performance through the effective rate meta-distribution, which accounts for the training overhead and beam misalignment errors. The results show the detrimental impact of misalignment errors when URLLC requirements are stringent and highlight the trade-off between the training overhead and the gain brought by multiple antennas. Insights are provided for optimally and jointly choosing the codebook size and the number of antennas.

Index Terms—Device-to-device, sidelink, stochastic geometry, beamforming, meta-distribution, misalignment, URLLC

I. INTRODUCTION

Device-to-Device (D2D) communication is one of the key technologies for future wireless and cellular networks. D2D indeed provides an efficient and reliable way for devices to communicate with each other, possibly without the assistance of a cellular infrastructure [1]. Compared to traditional communications via a Base Station (BS), D2D communications have numerous advantages such as increasing the overall network capacity, increasing the data rate or reducing latency thanks to the proximity between devices. This makes D2D an interesting candidate technology for Ultra-Reliable Low Latency (URLLC) communications, one of the pillars of 5G New Radio and future generations [2]. Millimeter wave (mmWave)

D2D communication is a technology that uses high-frequency radio waves in the range 30-300 GHz for direct communications between devices. Compared to sub-6 GHz bands usually adopted for cellular communications, mmWaves offer very large bandwidths, allowing fast and reliable transmissions [3]. High carrier frequencies are however characterized by a very short coherence time and a predominant Line-of-Sight (LOS) propagation with high attenuation [4]. In order to overcome these challenging propagation conditions, it is necessary to equip devices with multiple antennas and to perform beamforming to enhance the signal strength and quality [5]. To fully exploit the beamforming gain, the beams of D2D devices need to be steered towards desired directions through a process called beam training. The success of beam training depends on several factors, including the channel conditions, the training procedure, or the codebook design. Misalignment errors may thus occur, which can lead to a degradation of the data transmission performance [6], in particular in the context of communications with low latency and high reliability requirements. To better understand these challenges and to guide protocol designs, our study proposes a theoretical analysis of the communication reliability in mmWave D2D networks in the context of URLLC. Our approach is based on stochastic geometry and leverages the notion of meta-distribution in order to capture the reliability requirement of URLLC. It takes into account beam misalignment errors due to the beam training process when using mmWaves and the fundamental trade-off between training overhead and data transmission reliability.

A. Related works

Stochastic geometry is a widely used mathematical tool for evaluating the coverage and rate performance of wireless networks, see e.g. [7]. While early studies on D2D focus on the average coverage probability among all users [8], it is essential in the context of URLLC to consider the distribution of the traditional performance metrics, to know for example the proportion of users meeting reliability requirements, as defined e.g. in [2]. To fully characterize the spatial distribution of the communication reliability, the meta-distribution concept can be leveraged [9]. Several studies in the literature in stochastic geometry have taken into account beamforming [10]–[16]. Among those that have computed the rate meta-distribution of mmWave D2D networks, such as [10], [11], [15], [16], several papers assume a perfect beam alignment and overlook

Copyright (c) 20xx IEEE. Personal use of this material is permitted. However, permission to use this material for any other purposes must be obtained from the IEEE by sending a request to pubs-permissions@ieee.org.

Y. Quan is with LTCL, Telecom Paris, Institut Polytechnique de Paris and Orange Labs (yibo.quan@telecom-paris.fr). M. Coupechoux is with LTCL, Telecom Paris, Institut Polytechnique de Paris (marceau.coupechoux@telecom-paris.fr). J.M. Kélif is with Orange Labs (jeanmarc.kelif@orange.com). This work has been performed at LINC Laboratory. Part of this paper has been presented in the conference IEEE Globecom 2022.

the significance of beam misalignment. However, the effects of beam misalignment need to be studied as they play a crucial role in the network's performance. Some papers investigate the effects of beam misalignment, however in an incomplete way. This is the case for example of [12], [14], where the alignment errors are modelled using Gaussian or Uniform distributions. In [12], only the *average* coverage probability is derived. In [14], beam misalignment is taken into account in numerical results but not in the calculation of the meta-distribution. In our previous work [13], we approximate the meta-distribution for the mmWave D2D network with imperfect beam alignment by considering a Gaussian distributed alignment error while assuming Rayleigh fading channels. These approaches need to be extended to Nakagami-M fading channels, which are better suited to the prominent LOS propagation of mmWaves and include Rayleigh, Rician and more general fading distributions [17]. They also need to be extended to realistic misalignment error models derived from the alignment procedure. In order to better model the effect of beam misalignment, several papers analyse the beam training process [18]–[22]. These works assume an exhaustive search procedure, known as beam sweeping, to sequentially compare all possible transmitter-receiver beam directions. Specifically, the authors of [18], [19] study the impact of noise and derive upper and lower bounds for the misalignment probability. These studies are performed for a point-to-point transmission, while stochastic geometry allows for a system level analysis. Two papers are analysing beam misalignment in a cellular network context. Reference [21] studies the impact of user mobility, while the authors of [22] consider the potential beam misalignment due to the reuse of pilot signals by BSs. However, none of these works considers the effect of the codebook resolution, of the fast variation of the channel at mmWave frequencies and none of them studies the effective rate meta-distribution, a useful metric for URLLC. At last, several works have investigated the joint design of beam training and data transmission using stochastic geometry, see e.g. [20]–[22]. During the beam training process, there is indeed a fundamental trade-off between training and data transmission: Inadequate training may lead to poor channel estimation and thus to reduced data rate, while excessive training can result in disproportionate overhead. Reference [20] is focusing on mis-detection rather than on misalignment as the users always points to the sector with minimum path-loss. The authors of [22] ignore the possibility to have sub-optimal beam pairs (the joint beam gain is either maximal or zero). Reference [21] studies the overhead due to beam handovers and misalignment when a user is moving in the network. The authors however assume that beam alignment can always be completed within a fixed amount of time, ignoring the different time constraints for beam sweeping with different beam widths and potential misalignment due to inadequate training. Furthermore, these studies assume a perfect codebook, where beams perfectly span the angular aperture without any hole or overlapping between the beams. Side-lobes are also neglected. In practice, however, the codebook resolution plays an important role in the magnitude of the misalignment error. In these studies, Rayleigh fading is always assumed, while Nakagami-M is more appropriate and

more generic. At last, all these works focus solely on the average coverage probability of the network, while the study of the meta-distribution is required for understanding network performance in a URLLC context. Finally, in our previous work [23], [24], we have studied the stability of a spatio-temporal model considering beam misalignment, however without providing the rate meta-distribution nor accounting for URLLC constraints.

B. Contributions

We propose an analytical methodology based on stochastic geometry to study the communication reliability of mmWave D2D networks. The main contributions of the paper are as follows.

- We propose closed-form formulas for the joint Probability Mass Function (PMF) of the antenna gains at the transmitter and the receiver resulting from the beam sweeping process, assuming any generic small-scale fading distribution, including Nakagami-M and any codebook resolution. In the literature, papers studying this problem ignore the effect of the varying small-scale fading, and the influence of the codebook resolution [18]–[22].
- We derive closed-form formulas for the moments of the meta-distribution of the effective rate assuming Nakagami-M fading, from which we can derive the beta approximation. This meta-distribution allows us to obtain statistical latency guarantees for URLLC communications. In the literature, authors either ignore misalignment errors or do not study the rate meta-distribution [20]–[22].
- Via numerical experiments, we highlight the trade-offs between training and data resources and between the number of antennas and misalignment errors. We are able to optimize the codebook size and the number of antennas. To the best of our knowledge, these trade-offs have not been studied in the literature using the meta-distribution while taking into account the codebook resolution.

II. SYSTEM MODEL

In this section, we introduce the network model and the codebook-based beamforming model.

A. Network model

We consider a mmWave D2D network as a classical bipolar network model, where the D2D transmitters form a homogeneous Poisson point process (PPP) Φ^T with intensity $\Lambda(dx) = \lambda \times dx$ in a 2-dimensional space \mathbb{R}^2 [7]. Each D2D transmitter is associated with a dedicated receiver and performs point-to-point data transmissions. The point process associated with the receivers is denoted by Φ^R . We assume that the D2D receivers are uniformly located on the circles around their dedicated transmitters, with a constant radius r . Such a process can be interpreted as a marked point process of Φ^T with independent random marks. Hence Φ^R is also a homogeneous PPP [25]. According to the Slivnyak-Mecke theorem, the statistical characteristics do not change for a PPP

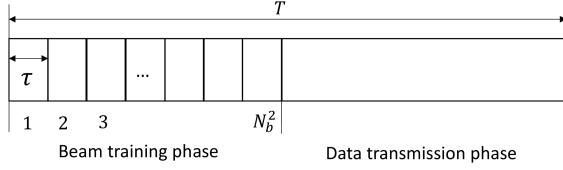


Fig. 1: Time slot of duration T made of: (i) A beam training phase, which consists of N_b^2 mini-slots of duration τ ; (ii) A data transmission phase.

if we add a typical point in a particular position, or more formally, the reduced Palm distribution $\mathbb{P}_x^1(\cdot)$ of Φ is equal to the original distribution $\mathbb{P}(\Phi \in \cdot)$ [26]. For convenience, a typical receiver is assumed to be located at the origin and attempts to receive the data from the corresponding transmitter. In order to compensate for the propagation loss of mmWaves, we consider that D2D transmitters and receivers are equipped with Uniform Antenna Arrays (ULA) with N_a antenna elements, which allow directional transmissions [27]–[29]. Every ULA can be configured with a codebook, which is a finite set of N_b possible beams pointing in directions that divide $[0, 2\pi)$ into equal intervals. We assume that all users are synchronized and that time is divided into slots of duration T , see Fig. 1. Each slot consists of a beam training phase and a data transmission phase. In the beam training phase, the transmitter and the receiver jointly train the beams from the pre-designed codebook. The beam training phase is divided into N_b^2 mini-slots of duration τ , during which every beam pair is measured before choosing the one providing the highest signal strength. During the data transmission phase, users employ the beam pair derived during the first phase to send a data file of size L bits. In the context of URLLC, the slot duration can be seen as a time budget that should be shared between the beam training and the data transmission of a small packet.

B. Beamforming and channel model

The channel is modelled with a distance dependent path-loss and small-scale fading. For a typical receiver located at a distance r from a transmitter, the path-loss is modelled as $\ell(r) = Kr^{-\alpha}$, where α is the path-loss exponent and K is a constant depending on the path-loss reference distance and the carrier frequency¹ [31]. The small scale fading coefficient h is modelled as a Nakagami-M fading, i.e., $h \sim \Gamma(M, \frac{1}{M})$ where Γ is the Gamma distribution with shape parameter M and rate parameter $\frac{1}{M}$ [17]. The special case $M = 1$ corresponds to Rayleigh fading. We denote $F(\cdot)$ and $f(\cdot)$ the Cumulative Distribution function (CDF) and the Probability Density Function (PDF) of h , respectively. The equivalent

¹We assume here a deterministic path-loss. Taking into account a probability to be in LOS which is decreasing with distance is left for future work. Analytical results can be however easily extended to the ball model considered in [10], [30].

channel matrix $\mathbf{H} \in \mathbb{C}^{N_a \times N_a}$, including the ULA responses, can be thus written as follows [32]:

$$\mathbf{H} = \sqrt{\ell(r)} \mathbf{h} \mathbf{u}(\psi) \mathbf{v}^*(\xi) \quad (1)$$

where $\mathbf{u}(\psi) \in \mathbb{C}^{N_a \times 1}$ and $\mathbf{v}(\xi) \in \mathbb{C}^{N_a \times 1}$ are the array response vectors at the receiver side and the transmitter side, respectively, ψ is the Angle-of-Arrival (AoA) and ξ is the Angle-of-Departure (AoD) of the plane wave with respect to the antenna arrays axis. This *single dominant path model* has been widely adopted by the literature on millimeter waves communications, see e.g. [33], [34]. The small scale fading coefficient is here due to non-resolvable multi-paths. Taking the phase at the first antenna element as a reference, the array response vectors can be expressed as follows [22]:

$$\mathbf{u}(\psi) = [1, e^{j\frac{2\pi d f_c}{c} \cos(\psi)}, \dots, e^{j\frac{2\pi d f_c}{c} (N_a - 1) \cos(\psi)}]^T \quad (2)$$

$$\mathbf{v}(\xi) = [1, e^{j\frac{2\pi d f_c}{c} \cos(\xi)}, \dots, e^{j\frac{2\pi d f_c}{c} (N_a - 1) \cos(\xi)}]^T \quad (3)$$

where d is the distance between the adjacent antenna elements, f_c is the carrier frequency and c is the speed of light. Each device can steer its antenna bore-sight towards its desired direction. The receiver steers the beam in direction θ^R with respect to the antenna array axis using a combining vector $\mathbf{w}(\theta^R)$. The transmitter steers the beam in direction θ^T with respect to the antenna array axis using a beamforming vector $\mathbf{f}(\theta^T)$. We have [29], [32]:

$$\mathbf{w}(\theta^R) = [1, e^{-j\frac{2\pi d f_c}{c} \cos(\theta^R)}, \dots, e^{-j\frac{2\pi d f_c}{c} (N_a - 1) \cos(\theta^R)}]^T \quad (4)$$

$$\mathbf{f}(\theta^T) = \frac{1}{\sqrt{N_a}} [1, e^{-j\frac{2\pi d f_c}{c} \cos(\theta^T)}, \dots, e^{-j\frac{2\pi d f_c}{c} (N_a - 1) \cos(\theta^T)}]^T \quad (5)$$

where the $\frac{1}{\sqrt{N_a}}$ factor is to account for the power split among the N_a antenna elements at the transmitter side. Ignoring for now interference, the received signal can be expressed as follows:

$$y = \mathbf{w}^*(\theta^R) \mathbf{H} \mathbf{f}(\theta^T) s + \mathbf{w}^*(\theta^R) \mathbf{z} \quad (6)$$

where s is the transmitted signal with average transmit power $\mathbb{E}[ss^*] = P$. The noise vector \mathbf{z} follows a circularly-symmetric complex normal distribution $\mathbf{z} \sim \mathcal{CN}(\mathbf{0}, \sigma^2 \mathbf{I})$ with average power $\sigma^2 = N_0 W$, where W is the signal bandwidth and N_0 is the Power Spectral Density (PSD) of thermal noise. The beamforming vector codebook is defined as $\mathcal{C}^T = \{\mathbf{f}(\theta_m^T)\}_{m=1:N_b}$, where $\theta_m^T = \frac{2\pi(m-1)}{N_b}$ and N_b is the size of the codebook, i.e., the number of possible beam directions. Respectively, we denote the combining vector codebook as $\mathcal{C}^R = \{\mathbf{w}(\theta_n^R)\}_{n=1:N_b}$, where $\theta_n^R = \frac{2\pi(n-1)}{N_b}$. Note that the sets $\{\theta_m^T\}_{m=1:N_b}$ and $\{\theta_n^R\}_{n=1:N_b}$ cover a full angle space of the transmitter and of the receiver respectively, with equal resolution $\theta_u = \frac{2\pi}{N_b}$. We denote $l = (m, n)$ a generic beamforming and combining vectors pair at transmitter and receiver sides, respectively. The small scale fading coefficients h are supposed to be independent and identically distributed (i.i.d.) for different beam pairs and between the training and the data transmission phases. This assumption is supported by the very short coherence time at high carrier frequencies. For example, assuming a speed of 10 km/h, the channel coherence time at 28 GHz is about 0.482 ms [4]. When the frequency

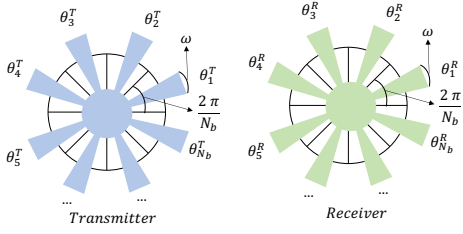


Fig. 2: Codebook and HPBW illustration.

is 71 GHz, the coherence time drops to 0.19 ms. These values are much shorter than a typical slot duration of 1 ms. Note that the equivalent antenna gains can be expressed as $g^T(\xi, \theta^T) = |\mathbf{v}^*(\xi)\mathbf{f}(\theta^T)|^2$ and $g^R(\psi, \theta^R) = |\mathbf{w}^*(\theta^R)\mathbf{u}(\psi)|^2$ at the transmitter and at the receiver, respectively. For tractability reasons, we approximate the actual antenna pattern by the widely used “flat-top” model [10], [21], [22]. This model consists of a main beam of angular aperture ω and a side beam of width $2\pi - \omega$. More precisely, the antenna gain of a transmitter can be expressed as:

$$g^T(\xi, \theta^T) = \begin{cases} G_{max}^T, & 0 \leq |\xi - \theta^T| \leq \omega/2 \\ G_{min}^T, & \text{otherwise.} \end{cases} \quad (7)$$

Accordingly, the antenna gain of a receiver $g^R(\psi, \theta^R)$ has a main lobe of gain G_{max}^R within the same angular aperture ω around its boresight direction θ^R , and a sidelobe of gain G_{min}^R outside this range. The main beam lobe width ω can be interpreted as the Half Power Beam Width (HPBW) of the antenna pattern. The main beam gain is precisely the maximum gain of the ULA. The side beam gain is obtained by normalizing the total radiation power.

Lemma 1: For a ULA with N_a antenna elements, the HPBW can be expressed as a function of N_a as follows:

$$\omega(N_a) = 2 \left(\frac{\pi}{2} - \arccos \frac{2.784}{N_a \pi} \right) \quad (8)$$

Furthermore, we have $G_{max}^T = N_a$, $G_{min}^T = \rho(N_a)$, $G_{max}^R = N_a^2$ and $G_{min}^R = N_a \rho(N_a)$, where

$$\rho(N_a) = \frac{\int_{-\pi}^{\pi} \frac{1}{N_a} \left| \frac{\sin(\frac{1}{2} N_a \pi \cos \theta)}{\sin(\frac{1}{2} \pi \cos \theta)} \right|^2 d\theta - N_a \omega(N_a)}{2\pi - \omega(N_a)} \quad (9)$$

Proof: See Appendix A. ■

The codebook parameters and the HPBW are illustrated in Fig. 2.

III. BEAM TRAINING AND MISALIGNMENT

We present here the beam training process and study the effects of beam misalignment.

A. Beam sweeping

During the beam training phase, the devices adopt a beam sweeping strategy where the transmitter and the receiver jointly steer the beams successively in a set of directions by adopting the beamforming/combining vectors pair from the

pre-defined codebooks presented in Section II-B. At every mini-slot of the training phase, the transmitter and its receiver choose a different beamforming and combining vectors pair $(f(\theta_m^T), w(\theta_n^R))$ from the codebooks $C^T \times C^R$, so that all pairs of vectors are measured. We denote $G_m^T = g^T(\xi, \theta_m^T)$ and $G_n^R = g^R(\psi, \theta_n^R)$ the transmitter and receiver antenna gains when the vectors pair $l = (m, n)$ is employed. The corresponding channel fading coefficient is denoted as h_l . The useful received signal when using the pair l is expressed as follows:

$$S_l = P h_l G_m^T G_n^R \ell(r) \quad (10)$$

After sweeping over all the codebooks vectors pairs, the transmitter and its receiver select the beamforming/combining vectors pair that maximizes S_l :

$$l^* = \arg \max_{\substack{l=(m,n) \\ m,n \in [1:N_b]}} S_l \quad (11)$$

The chosen vectors pair $l^* = (m^*, n^*)$ is then employed by users during the subsequent data transmission phase. The pair l^* is the best one during the training phase. As the channel power is varying due to fast fading, it is not necessary the best one during the data transmission phase. Received signal strengths are nevertheless correlated because the beam directions are kept constant for l^* between the training and the data transmission phases. The proposed procedure is inspired by the synchronization and cell selection procedure in 5G New Radio [35], [36]. The synchronization is indeed based on the measurement of the Reference Signal Received Power (RSRP) of the Secondary Synchronization Signal (SSS). The signal carried by the SSS has been designed such that any two different SSS have nearly optimal cross-correlation [37]. As a consequence, if devices use different SSS sequences (chosen for example at random while ignoring here possible collisions or pre-allocated), interference can be neglected during the beam sweeping phase.

B. Beam misalignment model

Beam misalignment may result from various phenomena like the device mobility, the resolution of the codebooks or the device phase errors [18], [19]. In this work, we consider the alignment errors induced during the training phase because of the codebook resolution and the channel variability. We assume the model shown in Fig. 3. A link between a typical D2D transmitter-receiver pair (in rose) is characterized by an AoA ψ_o and an AoD ξ_o . The transmitter and the receiver point their beam in the directions θ_T and θ_R , respectively ($\theta_T = \theta_R = \pi/2$ in the figure). The link between the typical receiver (‘RX’ in pink) and another interfering D2D device (‘TX’ in blue) located in x has an AoA ψ_x and an AoD ξ_x . A misalignment occurs when the transmitter beam direction is different from the AoD or when the receiver beam direction is different from the AoA, i.e., when either $e_T = |\xi_o - \theta_T|$ or $e_R = |\psi_o - \theta_R|$ are non zero. At the transmitter side for example, the maximum antenna gain is achieved as long as $e_T < \omega/2$, see (7). The error e_T may result from the codebook resolution: As θ_T takes values in a finite set, it may not

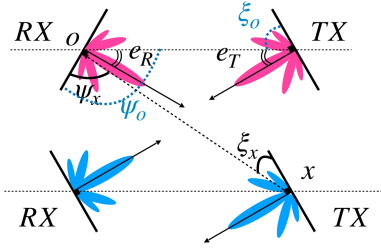


Fig. 3: A D2D transmitter-receiver (‘TX’ and ‘RX’ in pink) at the origin o characterized by an AoD ψ_o and an AoA ξ_o . The alignment errors are denoted as e_T and e_R . An interfering D2D transmitter-receiver pair (in blue) is located in x and is characterized by an AoA ψ_x and an AoD ξ_x with respect to the pink D2D pair.

coincide with the AoD ξ_o . The error may also result from channel variability: Due to the random variable h_l , the beam pair chosen during the training phase may not correspond to the best pair during the data transmission phase, see (10), (11). According to our network model, the AoD ξ_o and AoA ψ_o are uniformly distributed in $[0, 2\pi)$. Without loss of generality, we assume that the AoD and AoA correspond to the first value of the codebook, i.e., $\xi_o \in [\theta_1^T - \frac{\theta_u}{2}, \theta_1^T + \frac{\theta_u}{2})$ and $\psi_o \in [\theta_1^R - \frac{\theta_u}{2}, \theta_1^R + \frac{\theta_u}{2})$.

C. Probability mass function of antenna gains

During the beam sweeping phase, a transmitter and a receiver antenna gain G_m^T and G_n^R are respectively observed when the beam pair $l = (m, n)$ is measured. These antenna gains are i.i.d. random variables across the mini-slots due to the random AoA and AoD. The PMF of these antenna gains depends on the codebook resolution θ_u , the codebook size N_b and the HPBW ω . We derive this PMF in the following lemma.

Lemma 2: When $\omega \leq \theta_u$, the PMF of G_m^T can be expressed as follows:

$$\mathbb{P}[G_m^T = G_{max}^T] = \begin{cases} \frac{\omega}{\theta_u} & \text{if } m = 1 \\ 0 & \text{if } m \neq 1 \end{cases} \quad (12)$$

$$\mathbb{P}[G_m^T = G_{min}^T] = 1 - \mathbb{P}[G_m^T = G_{max}^T] \quad (13)$$

The PMF of G_n^R have similar expressions as in (12) and (13), where index n is replaced by m . When $\omega > \theta_u$, the PMF of G_m^T and G_n^R can be expressed as follows:

$$\mathbb{P}[G_m^T = G_{max}^T] = \begin{cases} 1 & \text{if } m \in I_1 \\ \frac{\text{mod}(\frac{\omega - \theta_u}{2}, \theta_u)}{\theta_u} & \text{if } m = \lfloor \frac{\omega - \theta_u}{2\theta_u} \rfloor + 2 \\ 0 & \text{if } m \in I_2 \\ \frac{\text{mod}(\frac{\omega - \theta_u}{2}, \theta_u)}{\theta_u} & \text{if } m = N_b - \lfloor \frac{\omega - \theta_u}{2\theta_u} \rfloor \\ 1 & \text{if } m \in I_3 \end{cases} \quad (14)$$

where $I_1 = [1 : \lfloor \frac{\omega - \theta_u}{2\theta_u} \rfloor + 1]$, $I_2 = [\lfloor \frac{\omega - \theta_u}{2\theta_u} \rfloor + 3 : N_b - \lfloor \frac{\omega - \theta_u}{2\theta_u} \rfloor - 1]$ and $I_3 = [N_b + 1 - \lfloor \frac{\omega - \theta_u}{2\theta_u} \rfloor : N_b]$.

$$\mathbb{P}[G_m^T = G_{min}^T] = 1 - \mathbb{P}[G_m^T = G_{max}^T] \quad (15)$$

The PMF of G_n^R have similar expressions as in (14) and (15), where index n is replaced by m .

Proof: See Appendix B. ■

During the data transmission phase, the beam pair $l^* = (m^*, n^*)$ has been chosen. The observed antenna gains $G_{m^*}^T$ and $G_{n^*}^R$ thus depend on the measurements performed during the beam sweeping phase. The total antenna gain for a typical link is their product. We provide hereafter their joint PMF.

Lemma 3: Let $\nu \in \mathcal{G}^T = \{G_{max}^T, G_{min}^T\}$ and $\kappa \in \mathcal{G}^R = \{G_{max}^R, G_{min}^R\}$ two possible values for the transmitter and receiver antenna gain, respectively. The joint probability $\mathbb{P}[G_{m^*}^T = \nu, G_{n^*}^R = \kappa]$ can be computed as follows:

$$\mathbb{P}[G_{m^*}^T = \nu, G_{n^*}^R = \kappa] = \sum_{\substack{m \in [1:N_b] \\ n \in [1:N_b]}} \mathbb{P}[G_m^T = \nu, G_n^R = \kappa, l^* = (m, n)] \quad (16)$$

where

$$\begin{aligned} & \mathbb{P}[G_m^T = \nu, G_n^R = \kappa, l^* = (m, n)] \\ &= \sum_{\substack{(\nu_i, \kappa_j) \in \mathcal{G}^T \times \mathcal{G}^R \\ i \in [1:N_b] \setminus m, j \in [1:N_b] \setminus n}} \{ \mathbb{E}_h [\prod_{\substack{\tilde{m} \in [1:N_b], \tilde{n} \in [1:N_b] \\ (\tilde{m}, \tilde{n}) \neq (m, n) \\ \nu_{\tilde{m}} = \nu, \kappa_{\tilde{n}} = \kappa}} F \left(\frac{h\nu\kappa}{\nu_{\tilde{m}}\kappa_{\tilde{n}}} \right)] \right. \\ & \left. \mathbb{P}[G_m^T = \nu] \mathbb{P}[G_n^R = \kappa] \prod_{\substack{i \in [1:N_b] \setminus m \\ j \in [1:N_b] \setminus n}} \mathbb{P}[G_i^T = \nu_i] \mathbb{P}[G_j^R = \kappa_j] \right\} \end{aligned} \quad (17)$$

where h is the channel fading coefficient with CDF $F(\cdot)$ and where the terms $\mathbb{P}[G_i^T = \nu_i]$ and $\mathbb{P}[G_j^R = \kappa_j]$ can be computed thanks to Lemma 2.

Proof: See Appendix C. ■

When $\omega < \theta_u$, there is no overlap between adjacent beams. As it can be seen in (12), the probability that G_1^T is equal to its maximum, G_{max}^T , increases when θ_u tends to ω . When $\omega > \theta_u$, the antenna beam can cover multiple sectors of width θ_u . A smaller θ_u allows for more sectors to be covered, all of which with a maximum antenna gain. Considering these two facts, as θ_u decreases, the probability that the chosen beam pair exhibits the maximum antenna gain increases, as it is shown in Lemma 3. Note that contrary to what is done in the literature [20], [22], we do not propose a misalignment probability but the complete PMF of joint antenna gain resulting from the training process.

IV. DATA TRANSMISSION

We characterize in this section the data transmission performance in a URLLC context.

A. Effective Achievable Rate and Delay

The transmission rate for a transmitter-receiver pair during the data transmission phase is approximated by the classical Shannon formula, where the interference is considered as noise [17]. For a typical receiver at origin o and its associated transmitter (see Fig. 3), the Signal to Interference plus Noise Ratio (SINR) is expressed as follows:

$$\gamma = \frac{Ph_{x_o} G_{m^*}^T G_{n^*}^R \ell(r)}{\sum_{x \in \Phi \setminus x_o} Ph_x g^R(\psi_x, \theta_{n^*}^R) g^T(\xi_x, \theta_{m^*}^T) \ell(|x|) + N_0 W} \quad (18)$$

and the *Transmission Rate* \mathcal{R} during the data transmission phase is expressed as follows:

$$\mathcal{R} = W \log_2(1 + \gamma) \quad (19)$$

where h_{x_o} and h_x are independent fading coefficients for the transmission and the interference link, respectively. The bore-sight direction of the interfering antenna is denoted θ_x^T . The antenna gains $G_{m^*}^T$ and $G_{n^*}^R$ are random variables following the PMF derived in Lemma 3. During the data transmission phase, a user sends a data file using the beam pairs $l^* = (m^*, n^*)$ chosen during the beam training phase. In order to account for the fraction of the slot dedicated to beam training, we define the *Effective Achievable Rate* [21], [22]:

$$\tilde{\mathcal{R}} = \left(1 - \frac{N_b^2 \tau}{T}\right)^+ \mathcal{R} \quad (20)$$

where the superscript $+$ denotes the function $h^+ = \max(h, 0)$. The *delay* D to transfer a data packet of length L consists of both the beam training delay and the data transmission delay:

$$D = N_b^2 \tau + \frac{L}{\mathcal{R}} \quad (21)$$

Note that we have used the Shannon formula to approximate the transmission rate. An alternative would have been to consider the finite block-length regime [38]. However, due to the difficulty to derive closed-form formulas with this regime, we consider this regime in the section dedicated to numerical results, Section VI-G.

B. Conditional Effective Rate Coverage Probability

The *Rate Coverage Probability*, $p_c(\eta)$, is defined as the probability that the transmission rate for a typical transmitter-receiver link is greater than a threshold η in bits/s.

$$p_c(\eta) = \mathbb{P}(\mathcal{R} > \eta) \quad (22)$$

This metric can only characterize the spatial average coverage performance among different users. Users at different locations however perceive different channel conditions, so that the coverage probability is itself random across the links. The *Conditional Rate Coverage Probability*, $P_c(\eta)$, has thus been introduced in [9] to characterize the reliability for a typical user given a specific network topology realization:

$$P_c(\eta) \triangleq \mathbb{P}(\mathcal{R} > \eta | \Phi^T, \Phi^R) \quad (23)$$

The rate coverage probability in (22) is nothing else than its expectation with respect to the processes $\{\Phi^T, \Phi^R\}$. In the same way, we define the *Conditional Effective Rate Coverage Probability* $\tilde{P}_c(\tilde{\eta})$, which is related to the effective achievable rate:

$$\tilde{P}_c(\tilde{\eta}) = \mathbb{P}\left(\tilde{\mathcal{R}} > \tilde{\eta} | \Phi^T, \Phi^R\right) \quad (24)$$

where $\tilde{\eta}$ is the effective rate threshold.

We define the *Conditional Success Transmission Probability* as the probability that the delay D is smaller than the slot duration T for a typical D2D pair:

$$\mathbb{P}(D < T | \Phi^T, \Phi^R) = \mathbb{P}\left(\mathcal{R} > \frac{L}{T - N_b^2 \tau} | \Phi^T, \Phi^R\right) \quad (25)$$

$$= \mathbb{P}\left(\tilde{\mathcal{R}} > \frac{L}{T} | \Phi^T, \Phi^R\right) \quad (26)$$

Equation (26) shows that when $\tilde{\eta} = \frac{L}{T}$, the conditional effective rate coverage probability is exactly the conditional success transmission probability to transfer a file of size L within a slot duration T . This is also equal to the rate coverage probability with $\eta = \frac{L}{T - N_b^2 \tau}$ during the data transmission phase, where $N_b^2 \tau \leq T$. In order to take into account the reliability requirements of URLLC, we now leverage the notion of meta-distribution.

C. Effective Rate Meta-distribution

The SINR, the rate and the effective rate depend on two sets of random variables, namely the point processes Φ^T and Φ^R on the one hand, all fading channels h_x on the other hand. The classical coverage probability in (22) provides an average over all sources of randomness but fails to describe the dispersion of the coverage probability across the links for a given point process realization. Yet, URLLC requirements in terms of latency and reliability should be achieved for a high proportion of users. We thus rely on the meta-distribution concept that decomposes the different sources of randomness and provides the proportion of links with a high coverage probability. The meta-distribution is defined as the complementary cumulative distribution function (CCDF) of the conditional coverage probability [9]. This metric provides the proportion of users whose coverage probability is above a certain threshold. It can thus be interpreted as a measure of the link reliability across the network. Similar to the definition in [9], [11], we define the *Rate Meta-distribution* to characterize the spatial distribution of the device communication reliability:

$$\bar{F}_{P_c(\eta)}(\epsilon) \triangleq \mathbb{P}^!(P_c(\eta) > \epsilon), \quad \epsilon \in [0, 1], \eta \in \mathbb{R}^+. \quad (27)$$

where $\mathbb{P}^!$ denotes the Palm measure of $\{\Phi^T, \Phi^R\}$. Respectively, this idea can be further extended to analyze the *Effective Rate Meta-distribution* as follows:

$$\bar{F}_{\tilde{P}_c(\tilde{\eta})}(\epsilon) \triangleq \mathbb{P}^!(\tilde{P}_c(\tilde{\eta}) > \epsilon), \quad \epsilon \in [0, 1], \tilde{\eta} \in \mathbb{R}^+. \quad (28)$$

Users can successfully complete transmission within the time slot T if the effective achievable rate exceeds $\tilde{\eta} = \frac{L}{T}$. In such cases, the effective rate meta-distribution provides the proportion of users whose probability of successful transmission is greater than ϵ . Communication is considered reliable when a typical user's probability of achieving a transmission rate higher than $\tilde{\eta}$ is greater than ϵ . We call ϵ the *Reliability Threshold* of the network.

V. RATE META-DISTRIBUTION WITH MISALIGNMENT

This section provides mathematically tractable expressions for the rate meta-distribution. A common approach involves first the derivation of the moments of the conditional coverage probability, and then the application of either the Gil-Pélaez theorem or the beta approximation [9].

A. Moments of the conditional rate coverage probability

Theorem 4: Consider a D2D network with the model introduced in Section II. The b -th moment of the conditional rate coverage probability $M_b(\eta) = \mathbb{E}[(P_c(\eta))^b]$ during the data transmission phase can be approximated as follows:

$$M_b \simeq \sum_{k_1+\dots+k_M=b} \binom{b}{k_1\dots k_M} \left(\prod_{m=1}^M \binom{M}{m} (-1)^{m+1} \right)^{k_m} \mathbb{E}_{G_o} \left[e^{-M\beta\eta' \frac{N_0W}{PG_o} \sum_{m=1}^M m k_m} e^{-\lambda Q(\eta', G_o)} \right] \quad (29)$$

where $\eta' = \frac{2\bar{W}-1}{\ell(r)}$, $\beta = [\Gamma(1+M)]^{-1/M}$, the term $\binom{b}{k_1\dots k_M}$ is the multinomial coefficient [39], and the variable $G_o = G_{m^*}^T G_{n^*}^R$ is the total antenna gain of the typical transmitter-receiver link. The function $Q(\eta', G_o)$ is defined as follows:

$$Q(\eta', G_o) = \frac{1}{2\pi} [\omega^2 A(\eta', G_o, G_{max}^T G_{max}^R) + \omega(2\pi - \omega) A(\eta', G_o, G_{max}^T G_{min}^R) + \omega(2\pi - \omega) A(\eta', G_o, G_{min}^T G_{max}^R) + (2\pi - \omega)^2 A(\eta', G_o, G_{min}^T G_{min}^R)] \quad (30)$$

where

$$A(\eta', G_o, G_x) = \lim_{T \rightarrow \infty} \frac{T^\delta \delta}{2} \int_0^1 \left(1 - \prod_{m=1}^M \left(1 + \frac{m\beta\eta' G_x}{G_o T t} \right)^{-M k_m} \right) t^{\delta-1} dt \quad (31)$$

and $\delta = 2/\alpha$.

Proof: See Appendix D. ■

Note that the PMF of $G_o = G_{m^*}^T G_{n^*}^R$ derived in Lemma 3 can be used to evaluate the expectation in (29) using the expression $\mathbb{E}_{G_o}[f(G_o)] = \sum_{\nu \in \mathcal{G}^T, \kappa \in \mathcal{G}^R} f(\nu\kappa) \sum_{m,n} \mathbb{P}[G_m^T = \nu, G_n^R = \kappa, l^* = (m, n)]$ for any function f .

An alternative expression for (31) is (see the details of the proof in Appendix D):

$$A(\eta', G_o, G_x) = \int_0^\infty \left(1 - \prod_{m=1}^M \left(1 + \frac{m\beta\eta' G_x \ell(|v|)}{G_o} \right)^{-M k_m} \right) v dv \quad (32)$$

Corollary 1: The first moment of the conditional coverage probability can be expressed as follows:

$$M_1 \simeq \sum_{m=1}^M \binom{M}{m} (-1)^{m+1} \mathbb{E}_{G_o} \left[e^{-mM\beta\eta' \frac{N_0W}{PG_o}} e^{-\lambda Q_1(m, \eta', G_o)} \right] \quad (33)$$

where the expression of $Q_1(m, \eta', G_o)$ is defined as follows:

$$Q_1(m, \eta', G_o) = \frac{1}{2\pi} [\omega^2 A_1(m, \eta', G_o, G_{max}^T G_{max}^R) + \omega(2\pi - \omega) A_1(m, \eta', G_o, G_{max}^T G_{min}^R) + \omega(2\pi - \omega) A_1(m, \eta', G_o, G_{min}^T G_{max}^R) + (2\pi - \omega)^2 A_1(m, \eta', G_o, G_{min}^T G_{min}^R)] \quad (34)$$

The function $A_1(m, \eta', G_o, G_x)$ can be expressed as follows:

$$A_1(m, \eta', G_o, G_x) = \lim_{T \rightarrow \infty} \frac{T^\delta}{2} \sum_{n=1}^M \binom{M}{n} (-1)^{n+1} {}_2F_1(n, \delta, \delta + 1; -\frac{G_o T}{m\beta\eta' G_x}) \quad (35)$$

where $B(\cdot)$ denotes the Beta function and ${}_2F_1(\cdot)$ denotes the hypergeometric function [40].

Proof: See Appendix D. ■

An alternative expression for (35) is:

$$A_1(m, \eta', G_o, G_x) = \int_0^\infty \left(1 - \left(1 + \frac{m\beta\eta' G_x \ell(|v|)}{G_o} \right)^{-M} \right) v dv \quad (36)$$

Setting $M = 1$ and owing to the monotonicity properties of the hypergeometric function, we can easily observe from (33) that the average coverage probability is an increasing function of the signal to noise ratio $\frac{PG_o}{N_0W}$, of the path-gain $\ell(r)$ between the transmitter and the receiver and a decreasing function of the threshold η , which confirms the intuition.

Corollary 2: The second moment of the conditional coverage probability can be expressed as follows:

$$M_2 \simeq \sum_{m=1}^M \binom{M}{m}^2 \times \mathbb{E}_{G_o} \left[e^{-2mM\beta\eta' \frac{N_0W}{PG_o}} e^{-\lambda Q_{21}(m, \eta', G_o)} \right] + \sum_{i=1}^{M-1} \sum_{j=i+1}^M 2 \binom{M}{i} \binom{M}{j} (-1)^{i+j} \times \mathbb{E}_{G_o} \left[e^{-(i+j)M\beta\eta' \frac{N_0W}{PG_o}} e^{-\lambda Q_{22}(i, j, \eta', G_o)} \right] \quad (37)$$

where functions $Q_{21}(m, \eta', G_o)$ and $Q_{22}(i, j, \eta', G_o)$ are defined as follows:

$$Q_{21}(m, \eta', G_o) = \frac{1}{2\pi} [\omega^2 A_{21}(m, \eta', G_o, G_{max}^T G_{max}^R) + \omega(2\pi - \omega) A_{21}(m, \eta', G_o, G_{max}^T G_{min}^R) + \omega(2\pi - \omega) A_{21}(m, \eta', G_o, G_{min}^T G_{max}^R) + (2\pi - \omega)^2 A_{21}(m, \eta', G_o, G_{min}^T G_{min}^R)] \quad (38)$$

$$Q_{22}(i, j, \eta', G_o) = \frac{1}{2\pi} [\omega^2 A_{22}(i, j, \eta', G_o, G_{max}^T G_{max}^R) + \omega(2\pi - \omega) A_{22}(i, j, \eta', G_o, G_{max}^T G_{min}^R) + \omega(2\pi - \omega) A_{22}(i, j, \eta', G_o, G_{min}^T G_{max}^R) + (2\pi - \omega)^2 A_{22}(i, j, \eta', G_o, G_{min}^T G_{min}^R)] \quad (39)$$

and $A_{21}(m, \eta', G_o, G_x)$ and $A_{22}(i, j, \eta', G_o, G_x)$ are defined as:

$$A_{21}(m, \eta', G_o, G_x) = \lim_{T \rightarrow \infty} \frac{T^\delta}{2} \sum_{n=1}^{2M} \binom{2M}{n} (-1)^{n+1} {}_2F_1(n, \delta, \delta + 1; -\frac{G_o T}{m\beta\eta' G_x}) \quad (40)$$

$$A_{22}(i, j, \eta', G_o, G_x) = \lim_{T \rightarrow \infty} \frac{T^\delta \delta}{2} \int_0^1 \left(1 - \left(1 + \frac{i\beta\eta' G_x}{G_o T t} \right)^{-M} \left(1 + \frac{j\beta\eta' G_x}{G_o T t} \right)^{-M} \right) t^{\delta-1} dt \quad (41)$$

Proof: See Appendix D. ■

Alternative expressions of (40) and (41) are:

$$A_{21}(m, \eta', G_o, G_x) = \int_0^\infty \left(1 - \left(1 + \frac{m\beta\eta' G_x \ell(|v|)}{G_o} \right)^{-2M} \right) v dv \quad (42)$$

$$A_{22}(i, j, \eta', G_o, G_x) = \int_0^\infty \left(1 - \left(1 + \frac{i\beta\eta' G_x \ell(|v|)}{G_o} \right)^{-M} \left(1 + \frac{j\beta\eta' G_x \ell(|v|)}{G_o} \right)^{-M} \right) v dv \quad (43)$$

We have noticed that formulations (31), (35), (40), and (41) accelerate the convergence of the numerical evaluation when T is increasing with respect to their infinite integral counterparts (32), (36), (42), and (43).

Corollary 3: To calculate the b -th moment of the conditional effective rate coverage probability $\tilde{P}_c(\tilde{\eta})$ in (24), we only need to replace η in Theorem 4 by $\frac{T\tilde{\eta}}{T - N_b^2 \tau}$, where $N_b^2 \tau < T$.

B. Beta approximation

The numerical computation of the exact rate meta-distribution by using Gil-Pélaez theorem is often difficult. An alternative solution is to approximate it with a beta distribution by matching the first and the second moment as follows:

$$\tilde{F}_{P_c(\eta)}(\epsilon) = 1 - I_\epsilon \left(\frac{M_1 M_2 - M_1^2}{M_1^2 - M_2}, \frac{(1 - M_1)(M_2 - M_1)}{M_1^2 - M_2} \right) \quad (44)$$

where $I_\epsilon(\cdot)$ is the regularized incomplete beta function [10]. Similarly the effective rate meta-distribution $\tilde{F}_{\tilde{P}_c(\tilde{\eta})}(\epsilon)$ can be approximated by using the first and second moment of $\tilde{P}_c(\tilde{\eta})$.

VI. NUMERICAL RESULTS

This section aims at verifying the accuracy of our analytical approximation through Monte Carlo simulations and providing insights for the design of mmWave URLLC D2D networks.

A. Simulation settings

Our simulation settings are close to the synchronization and initial access process parameters defined for 5G New Radio (NR) [41]. Our simulations assume a carrier frequency of $f_c = 28$ GHz and a transmission bandwidth of $W = 400$ MHz [42]. We assume a mini-slot duration of $\tau = 4.46 \mu\text{s}$, which is equivalent to one orthogonal frequency-division multiplexing (OFDM) symbol time with cyclic prefix, given a sub-carrier

TABLE I: System Parameters

Symbol	Description	Default values
W	Transmission bandwidth	400 MHz
P	Transmit power	28 dBm
N_0	Thermal noise PSD	-166 dBm/Hz
r	The link distance between D2D users	30 m
f_c	Carrier frequency	28 GHz
K	FSPL at reference distance 1 m	$7.2695e - 07$
α	Path-loss exponent	2.3
T	Time slot duration	1 ms
τ	Mini-slot time duration	$4.46 \mu\text{s}$
L	File size	32 bytes
λ	D2D transmitter-receiver pairs density	0.001 m^{-2}
M	Nakagami-M shape parameter	3

spacing of 240 kHz [42]. Inspired by URLLC requirements, we set $T = 1$ ms and $L = 32$ bytes [43]. Path-loss parameters are derived from the micro-cell scenario in [43]. The path-loss exponent is taken from [31]; the constant path-gain K is calculated as the free space path loss (FSPL) at a reference distance of 1 meter, which is equal to $(\frac{c}{4\pi f_c})^2$, where c is the speed of light. The distance between a receiver and its associated transmitter is set to $r = 30$ m, with a transmission power of $P = 28$ dBm. The noise PSD is $N_0 = -174 + \text{NF}$ dBm/Hz where the noise factor is set to $\text{NF} = 8$ dB. We assume a transmitter-receiver pair intensity of $\lambda = 0.001 \text{ m}^{-2}$ by default, i.e., the average distance between neighboring transmitter-receiver pairs is around 30 m. We consider between 2 and 10 antennas, which are typical values for devices at millimeter waves [44], [45], [46], [47]. Parameters values are summarized in Tab. I. Monte Carlo simulations run over multiple snapshots. The original network area is a square of side length $L_n = 600$ m. Transmitters are drawn according to a Poisson process of intensity λ and receivers are located at distance r with a uniform orientation. In order to deal with border effects, we adopt a *torus network*, in which the original square network is surrounded by eight copies of it. The distance between a receiver and an interferer is computed as the minimum distance toward any of the copies. At every snapshot, a link coverage probability is computed by varying the fading channel. Statistics are recorded only in the central square network.

B. Beam misalignment

We illustrate here the probability mass function of the antenna gains as derived in Lemma 3. Fig. 4 shows three joint transmit and receive antenna gains probabilities as a function of the codebook size N_b for $N_a = 4$ antennas, namely $\mathbb{P}(G_{m^*}^T = G_{max}^T, G_{n^*}^R = G_{max}^R)$, $\mathbb{P}(G_{m^*}^T = G_{max}^T, G_{n^*}^R = G_{min}^R)$ and $\mathbb{P}(G_{m^*}^T = G_{min}^T, G_{n^*}^R = G_{min}^R)$, i.e., the probabilities that the beams are perfectly aligned, partly aligned or not aligned at all after the training phase. We first observe that simulation and analytical results match very well, which was expected as there is no approximation in the derivation of Lemma 3. When the codebook size is small, i.e., the training phase is short, complete misalignment dominates (see Fig. 4 (c)). When the codebook size is large, perfect beam alignment is the most probable event (see Fig. 4 (a)). In between, the training phase

increasingly finds a single maximum gain (for example here at the transmitter side) but not at both sides (see Fig. 4 (b)). The probability of finding a single maximum then decreases as perfect beam alignment becomes more probable.

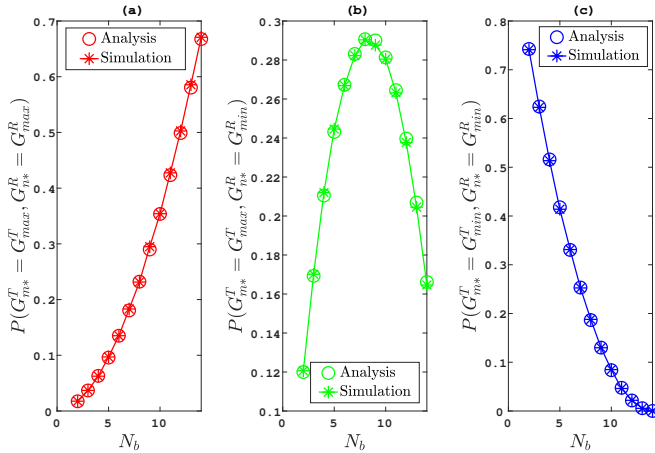


Fig. 4: Three probabilities derived from Lemma 3 as function of the codebook size N_b ($N_a = 4$).

C. Impact of the number of antennas on the transmission rate

We investigate here the impact of the number of antennas on the data transmission rate while keeping the codebook size fixed at $N_b = 15$. As a consequence, the same codebook and the same beam directions are used whatever the number of antennas. We set the transmission rate threshold to $\eta = \frac{L}{T}$. Fig. 5 (a) and (b) show the mean and the variance of the conditional rate coverage probability $P_c(\eta)$ as a function of the number of antennas N_a . The green curves show the analytical results, see (29), while the red curves depict the simulation results. Dashed curves assume a perfect alignment of the transmitter and receiver beams, i.e., $G_o = G_{max}^T G_{max}^R$ always holds in equations. We first see that analysis and simulation results match very well: this confirms the accuracy of our approximation of the lower incomplete gamma function, see (58). Fig. 5 (a) shows that the mean of the conditional rate coverage probability is a monotonically increasing function of N_a when the beam alignment is perfect. This was expected since an increase in the number of antennas results in a stronger main lobe gain and a narrower beamwidth ω of the main lobe. These effects lead to a higher received power and a weaker interference when there are no alignment errors. However, when considering the beam misalignment due to the training phase, the performance may degrade. In Fig. 5 (a), we see that the mean of the conditional rate coverage probability is first increasing and then decreasing with a maximum achieved for $N_a = 4$. Below this threshold, the amount of resources dedicated to training is sufficient and increasing the number of antennas also increases the joint antenna gain, leading in turn to better coverage. Beyond the optimal number of antennas however, the training phase is not sufficient for a good beam alignment: beams are thinner and even a small misalignment error leads to a rapid degradation of the coverage. This figure

highlights the trade-off between the number of antennas and the rate coverage in the presence of beam misalignment, a phenomenon that is not captured by studies assuming perfect beam alignment. Fig. 5 (b) shows the variance of $P_c(\eta)$ as a function of N_a . When there is no misalignment, the variance is monotonically decreasing with the number of antennas. As N_a is increasing, the transmit power is indeed more and more precisely focused on the transmitter-receiver link, so that the interference created to other D2D pairs decreases; D2D transmissions tend to be more and more independent of each others, so that the coverage performance is more homogeneous and the variance decreases. When misalignment errors are taken into account, the same trend is observed when the number of antennas is small because the training is sufficient to achieve a good alignment. On the contrary, when N_a grows, there are either very good communication conditions if beams manage to be aligned despite the poor training or very bad conditions when the error is significant. Thinner beams increase these differences, so that the variance increases. For a given reliability threshold ϵ , we can interpret the meta-distribution as the proportion $\bar{F}_{P_c(\eta)}(\epsilon)$ of users who meet the reliability requirement. In Fig. 5 (c) and (d), we compare the percentage of users who meet the reliability requirement assuming two reliability thresholds, namely $\epsilon = 0.9$ and $\epsilon = 0.99999$. The green curves in the figures depict the beta approximations for $\bar{F}_{P_c(\eta)}(\epsilon)$, while the red curves are obtained through simulations. The dashed curves are obtained from the beta approximation when the alignment is perfect. The figures demonstrate that the beta approximation is an accurate technique for analyzing the meta-distribution. The proportion of users meeting the reliability requirements follows the same trend as the mean of the conditional rate coverage probability for the same reasons: in absence of error, thinner beams provide enhanced signal strength, while in presence of errors, thinner beams are beneficial as long as the training resources are sufficient. There is thus an optimal number of antennas that maximizes the proportion of users meeting the reliability requirements. At last, changing the reliability threshold does not alter the performance trends, but it does impact the proportion of users that can satisfy the reliability constraint. For example, with 8 antennas, about 99.5% of the links can satisfy a reliability threshold of 90%, while only 97.5% of the links can achieve a more stringent reliability threshold of 99.999%.

D. Impact of the codebook size on the transmission rate

In addition to the number of antennas, the size of the training codebook, represented by the variable N_b , is another critical constraint that affects the network's performance. The transmission rate threshold is set to $\eta = \frac{L}{T}$. Fig. 6 (a) and (b) show the mean and the variance of the conditional rate coverage probability $P_c(\eta)$ as a function of N_b for different numbers of antennas. The solid curves represent analytical results obtained from (29) while the dashed curves have been obtained from simulations. The straight dotted lines have been obtained with a perfect beam alignment. Here again, we see that analysis and simulations match very well. This

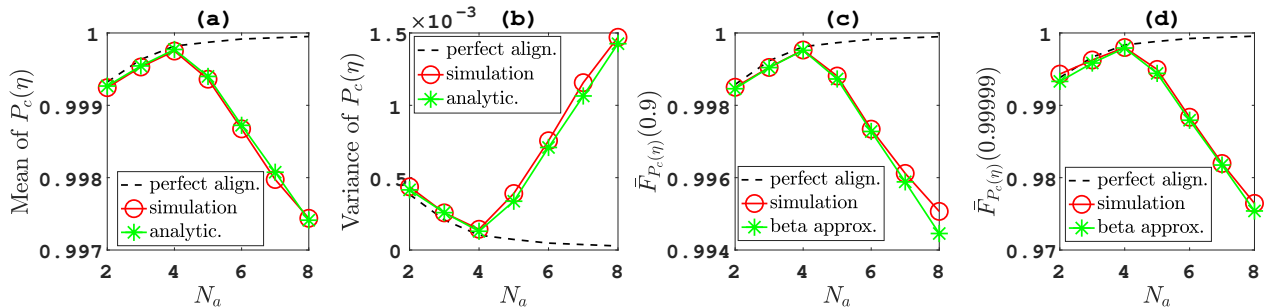


Fig. 5: Mean (a) and variance (b) of the conditional rate coverage probability; Proportion of links that have a conditional rate coverage probability greater than a reliability threshold of 90% (c) or 99.999% (d), as a function of the number of antennas.

confirms the tightness of our approximation. In both figures, we observe that the curves accounting for misalignment errors converge to the curves assuming perfect alignment. As N_b increases, the codebook resolution θ_u decreases, so that the transmitter and the receiver have a finer estimation of the AoA and AoD. The probability of having an alignment error decreases and the magnitude of this error is also decreasing. In a nutshell, the higher is N_b , the more accurate is the training period. After some threshold, however, increasing N_b does not provide a significant gain on the performance since the beam resolution is much lower than the beam width. The figure also demonstrates that if N_a is large, $P_c(\eta)$ requires a larger N_b to approach its limit, as more antennas with thinner beam lobes require codebooks with a more precise resolution to perform beam alignment. At last, we see that the variance is decreasing with N_b and increasing with N_a . This can be explained by the fact that misalignment errors introduce variability in the communication conditions across the links. Fig. 6 (c) illustrates the percentage of D2D users whose conditional rate coverage probability $P_c(\eta)$ is larger than the reliability threshold of $\epsilon = 99.999\%$ as a function of N_b . The dashed curves show simulation results, while the solid curves are obtained using the beta approximation. Again, the close agreement between the curves suggests that the beta approximation is an accurate tool for analyzing the meta-distribution. These curves exhibit the fact that a longer training time can better align the beams and enable more users to have reliable communications. Increasing the number of antennas can ultimately guarantee more users to meet the reliability requirement, but it requires longer training time. For example, if we want to achieve a reliability of 99.999% for more than 99% of the users, then a training period with $N_b = 7, 11,$ and 21 is required for $N_a = 2, 4,$ and 8 antennas, respectively. However, it is impossible to have more than 99.5% of the users meeting the reliability requirement with only $N_a = 2$ antennas as the performance is saturating to a lower value, whatever the training period.

E. Effective achievable rate analysis

The analysis presented so far focuses on the rate coverage probability during the data transmission phase. However, when taking into account the overhead of the beam training phase, the size of the beam training codebook is limited by the

total time budget, resulting in $N_b \leq \lfloor \sqrt{\frac{T}{\tau}} \rfloor$. In this section, we study the effective achievable rate with an effective rate threshold of $\tilde{\eta} = \frac{I}{T}$. Fig. 7 illustrates how the mean of the conditional effective rate coverage probability $\tilde{P}_c(\tilde{\eta})$ evolves with respect to N_b for different numbers of antennas. The solid curves represent analytical results obtained using the equations of Corollary 3, while the dashed curves depict simulation results. The dotted lines represent the conditional rate coverage probabilities when there is no misalignment. We first observe that the mean is decreasing with N_b in the absence of errors. This is due to the lack of data resources when the training period becomes longer and the trend is directly related to the first factor of (20). We then see that, in the presence of misalignment errors, curves are first increasing and then possibly decreasing. The reason lies in two conflicting effects: when N_b increases, the misalignment errors decrease while the amount of resources dedicated to data is reduced. Fig. 7 shows that an almost perfect alignment is achieved for $N_b = 7$ and 14 for $N_a = 2$ and 4 antennas, respectively. This means that no improvement can be expected from the training after these thresholds. This explains why the performance reaches its maximum at these values. On the contrary, for $N_a = 8$ antennas, the training is far from perfect when $N_b = 14$. The training is not able to compensate for the lack of data resources. Overall, $N_a = 2$ and $N_b = 8$, or $N_a = 4$ and $N_b = 14$ offer the best performance, while $N_a = 8$ antennas are not able to recover from the errors with reasonable overhead.

By fixing N_b to a low value, e.g. $N_b = 4$, Fig. 7 shows that $\tilde{P}_c(\tilde{\eta})$ decreases as the number of antennas increases. This is due to the imprecise resolution of the codebook and a severe beam misalignment. With more antennas, the beam width is thinner and misalignment worsens. When $N_b = 14$ on the contrary, $\tilde{P}_c(\tilde{\eta})$ reaches its maximum with 4 antennas, which offer the best trade-off between signal quality achieved with beamforming and misalignment errors induced by an incomplete training. Fig. 8 (a) shows the proportion of D2D users with a conditional effective rate coverage probability \tilde{P}_c above the threshold $\epsilon = 99.999\%$ as a function of N_b for the different number of antennas. The proportion $\bar{F}_{\tilde{P}_c(\tilde{\eta})}(\epsilon)$ is first increasing with N_b when N_b is small and then dropping quickly when $N_b^2 \tau$ approaches T . For a reliable URLLC network with low latency, a common requirement is that 95% of the users operate with 99.999% reliability and 1 ms latency

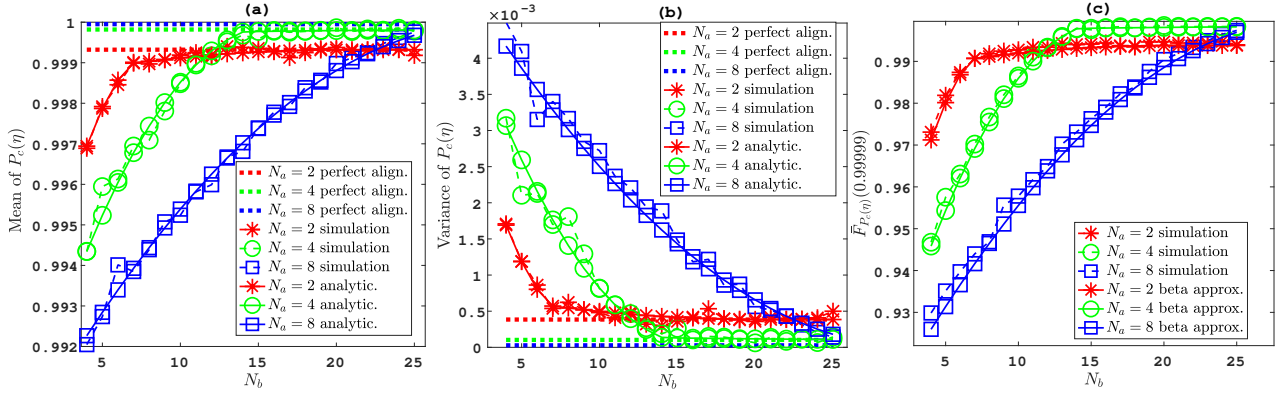


Fig. 6: Mean (a) and variance (b) of the conditional rate coverage probability; Proportion of links that have a conditional rate coverage probability greater than a reliability threshold of 99.999% (c), as a function of the number of beams.

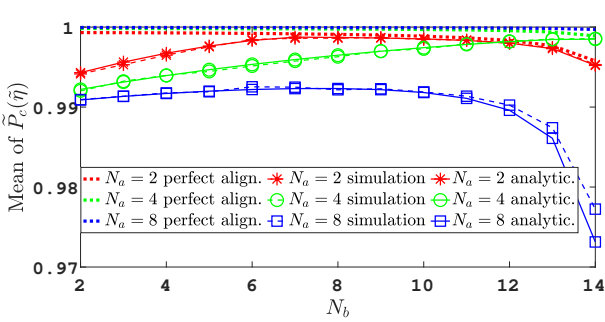


Fig. 7: Mean of the conditional effective rate coverage probability as a function of the number of beams.

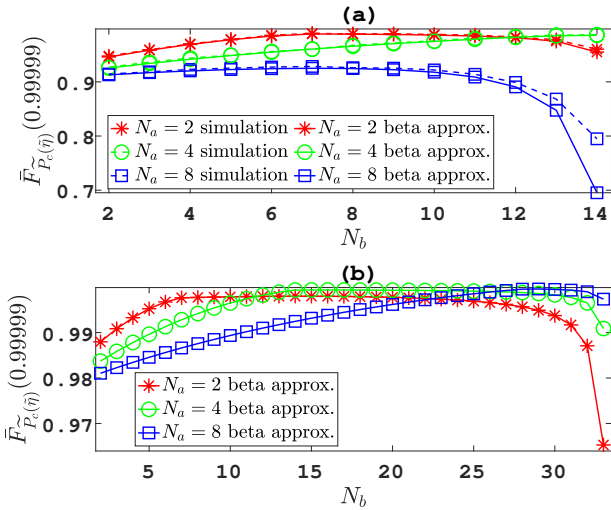


Fig. 8: Proportion of links with a conditional effective rate coverage probability greater than 99.999% as a function of the number of beams for $T = 1$ ms (a) and $T = 5$ ms (b).

[2]. According to Fig. 8 (a), $N_a = 2$ always meets this strict constraint. When $N_a = 4$, N_b needs to be larger than 5 to ensure the reliability requirement. On the contrary, $N_a = 8$ antennas cannot achieve it. However, increasing the number of antennas becomes a valid option if the delay requirement

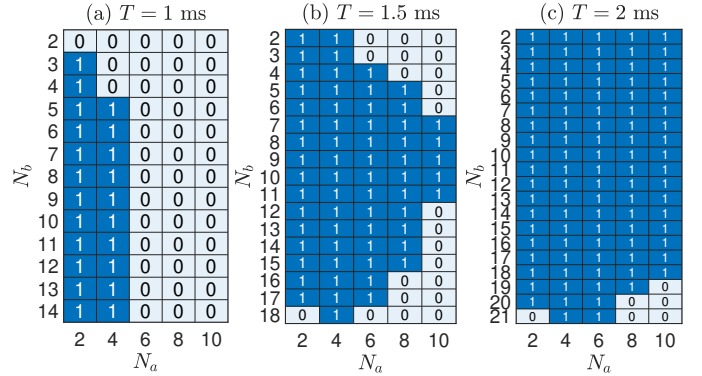


Fig. 9: Feasibility of the URLLC requirement that 95% of the users communicate with 99.999% reliability and 1 (a), 1.5 (b), and 2 ms (c) latency [2] (feasible combinations in dark blue).

is relaxed. In Fig. 8 (b), the slot duration is set to $T = 5$ ms. This lets more room for training and N_b can reach a higher value (here 33) on the x-axis. We see here how the optimal number of antennas varies with N_b . If N_b is small, it is better to use fewer antennas so that misalignment errors are less impactful. As N_b is increasing, it is more and more interesting to increase the number of antennas because we have enough time to train the beams, and consequently, the higher beam gains outperform the loss due to misalignment. For our studied scenario, the possible design choices in terms of the number of antennas and beams are summarized in Fig. 9 and 10. We see how relaxing the different constraints extends the possible network design choices. Note that this kind of result cannot be derived by using the standard coverage probability but necessitates the meta-distribution.

F. Impact of Nakagami- M shape parameter

The shape parameter M of the Nakagami- M fading channel characterizes the severity of the fading [17]. The case $M = 1$ corresponds to Rayleigh fading, while there is no fading when $M \rightarrow \infty$. An environment with a higher value of M is thus more favorable for the beam training process. This is illustrated in Fig. 11. When M is increasing, there are more links that can meet the reliability constraint. As the fading is

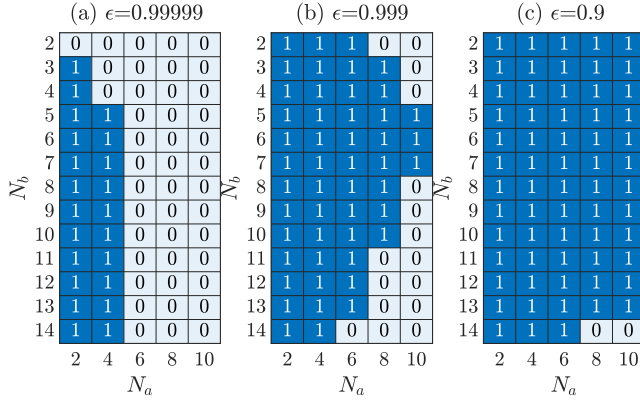


Fig. 10: Feasibility of the URLLC requirement that 95% of the users communicate with 99.999% (a), 99.9% (b), 90% (c) reliability and $T = 1$ ms latency (feasible combinations in dark blue).

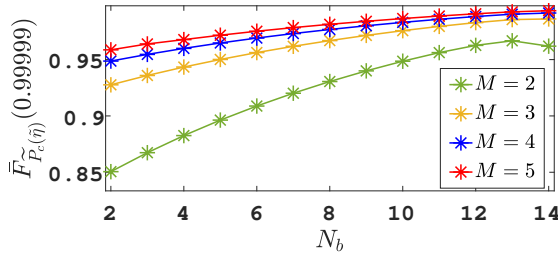


Fig. 11: Proportion of links with a conditional effective rate coverage probability greater than 99.999% ($N_a = 4$, $T = 1$ ms).

less severe, the channel can indeed be better predicted from the training phase. This confirms our initial analysis that channel fading plays a critical role in the beam training process.

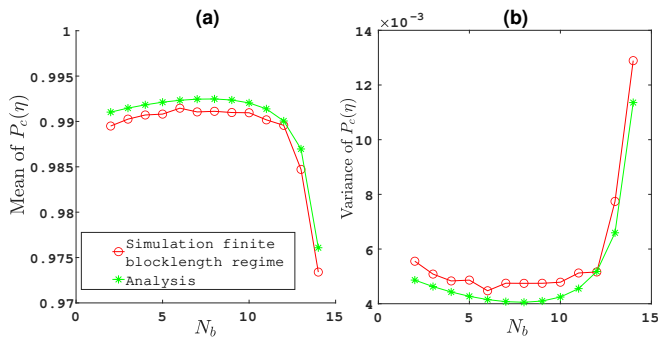


Fig. 12: Mean (a) and variance (b) of the conditional rate coverage probability - Analysis and simulation assuming a finite block length regime ($N_a = 8$, $\epsilon_c = 10^{-5}$).

G. Finite block length regime

The finite block-length regime [38] is sometimes adopted in the literature for the calculation of the achievable rate when URLLC is considered. In this case, the new *Effective*

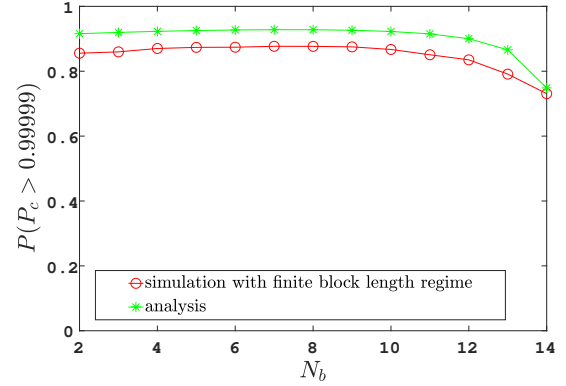


Fig. 13: Proportion of links that have a conditional rate coverage probability greater than 99.999% - Simulations assume a finite block length regime ($N_a = 8$, $\epsilon_c = 10^{-5}$).

Achievable Rate expression is given by (see [48] for a similar derivation):

$$\tilde{\mathcal{R}}^* = \left(1 - \frac{N_b^2 \tau}{T}\right)^+ W \left(C(\gamma) - \sqrt{\frac{V(\gamma)}{W(T - N_b^2 \tau)}} Q^{-1}(\epsilon_c) \right) \quad (45)$$

where ϵ_c is the message error probability, $C(\gamma) = \log_2(1 + \gamma)$, $V(\gamma) = \frac{\gamma}{2} \frac{\gamma+2}{(\gamma+1)^2} \log_2^2 e$ and $Q(x) = 1/\sqrt{2\pi} \int_x^\infty \exp(-t^2/2) dt$. The *Rate Coverage Probability* can be written as:

$$p_c(\eta) = \mathbb{P}(\tilde{\mathcal{R}}^* > \eta)(1 - \epsilon_c) \quad (46)$$

Other performance metrics can be redefined in the same way by taking into account ϵ_c and $\tilde{\mathcal{R}}^*$. However, it is an open problem to derive closed-form formulas in this context. In Figures 12-13, we show the mean and variance of the conditional rate probability and the proportion of links with a rate coverage probability greater than 99.999% obtained using our analytical formulas based on the Shannon formula and by simulations assuming a finite block length regime. We see that, although less accurate, our analytical study provides good approximations. More investigations are nevertheless required to develop an analytical study with more accurate results.

VII. CONCLUSION

We propose an analytical framework to investigate the impact of beam misalignment on mmWave URLLC D2D networks. First, the joint antenna gain distribution is evaluated based on the study of an imperfect exhaustive search approach. The imperfection of the beam sweeping procedure comes from the finite codebooks, the finite amount of resources dedicated to training and the high variability of the channel at high frequencies. We then derive mathematical expressions for the moments of the conditional effective rate coverage probability assuming Nakagami-M fading, and we approximate the effective rate meta-distribution using a beta approximation. Our results show that misalignment errors can be highly detrimental if URLLC requirements are stringent. Misalignment errors not only reduce the joint beam gain but also introduces variability in the link quality that affects reliability. At last, our study highlights the trade-off between the training overhead and

the number of antennas. Having fewer antennas is preferable when a very short delay is required with high reliability. The potential gain of many antennas can however be exploited when the delay constraint is relaxed.

APPENDIX

A. Proof of Lemma 1

Consider a ULA at the transmitter side with N_a equally spaced antenna elements. The corresponding array response vector is shown in (3). By choosing the beamforming vector shown in (5), the combined far field pattern $f_a^T(\xi, \theta^T) = \mathbf{v}^*(\xi)\mathbf{f}(\theta^T)$ of the array is obtained as:

$$f_a^T(\xi, \theta^T) = \frac{1}{\sqrt{N_a}} \sum_{i=1}^{N_a} e^{j((i-1)\frac{2\pi d f_c}{c}(\cos(\xi) - \cos(\theta^T)))} \quad (47)$$

The power gain $g^T(\xi, \theta^T) = |f_a^T(\xi, \theta^T)|^2$ leads to:

$$g^T(\xi, \theta^T) = \frac{1}{N_a} \left| \frac{\sin(N_a \frac{\pi d f_c}{c} (\cos(\xi) - \cos(\theta^T)))}{\sin(\frac{\pi d f_c}{c} (\cos(\xi) - \cos(\theta^T)))} \right|^2 \quad (48)$$

The maximum array factor gain is achieved when the steering direction and the AoD align: $\theta^T = \xi$. The maximum array factor at the transmitter side is $G_{max}^T = N_a$. We assume that $d = \frac{c}{2f_c}$ and the antenna is broadside ($\theta^T = \pi/2$) [29]. The half power beam width in (8) is obtained by solving the following equation:

$$\frac{1}{N_a} \left| \frac{\sin(\frac{1}{2}N_a\pi \cos(\pi/2 - \omega/2))}{\sin(\frac{1}{2}\pi \cos(\pi/2 - \omega/2))} \right|^2 = \frac{N_a}{2} \quad (49)$$

Let $K(N_a)$ be the total radiation power gain of the ULA:

$$K(N_a) = \int_{-\pi}^{\pi} \frac{1}{N_a} \left| \frac{\sin(\frac{1}{2}N_a\pi \cos(\xi))}{\sin(\frac{1}{2}\pi \cos(\xi))} \right|^2 d\xi \quad (50)$$

Let ρ be the minimum gain in the side lobe of transmitter. We equalize the approximate and exact radiated powers as follows and deduce the sidelobe gain:

$$N_a\omega(N_a) + \rho(N_a)(2\pi - \omega(N_a)) = K(N_a) \quad (51)$$

$$\rho(N_a) = \frac{K(N_a) - N_a\omega(N_a)}{2\pi - \omega(N_a)} \quad (52)$$

In a similar way, we get that the HBPW ω for the receiver antennas is the same as that at the transmitter end. The maximum gain of receiver antennas is N_a times that for the transmitter antenna. The minimum gain of receiver's antenna has the value $G_{min}^R = N_a\rho$.

B. Proof of Lemma 2

Let first notice that, as a receiver is uniformly distributed around its associated transmitters, the AoD ξ is uniformly distributed in $[0, 2\pi)$. Let also recall that, without loss of generality, the AoD corresponds to the first value of the codebook, i.e., $\xi \in [\theta_1^T - \frac{\theta_u}{2}, \theta_1^T + \frac{\theta_u}{2})$ which corresponds to $m = 1$ in the equations. Let first assume that $\omega \leq \theta_u$, i.e., the beamwidth is smaller than the codebook resolution. This means that the transmitter can achieve the maximum gain only

when it is pointing in the direction $m = 1$. As a consequence, $\mathbb{P}[G_m^T = G_{max}^T] = 0$ when $m \neq 1$. When $m = 1$, the maximum gain is achieved with probability $\frac{\omega}{\theta_u}$ owing to the uniform distribution of the AoD. This proves equations (12) and (13). Let's now consider the case $\omega > \theta_u$, i.e., the beamwidth is larger than the codebook resolution. In this case, some sectors are fully covered by the beam, some are partially covered and some are not covered. This corresponds to the different sub-cases of (14). The probabilities are related to whether or not the first sector is fully covered, partially covered or not covered by the beam. The beam fully covers $2\lfloor \frac{\omega - \theta_u}{2\theta_u} \rfloor$ adjacent sectors of size θ_u . Thus, the first sector $m = 1$ is fully covered if the transmitter points towards a sector $m \in I_1$ or $m \in I_3$. When the first sector is fully covered, the probability to achieve the maximum gain is one because we have assumed that the AoD falls in this sector. In addition to the fully covered sectors, there are two additional sectors at the margins of the beam that are partially covered. The first sector is one of them if $m = \lfloor \frac{\omega - \theta_u}{2\theta_u} \rfloor + 2$ or $m = N_b - \lfloor \frac{\omega - \theta_u}{2\theta_u} \rfloor$. In this case, owing to the uniform distribution of the AoD, the maximum gain is achieved with probability $\frac{\text{mod}(\frac{\omega - \theta_u}{2}, \theta_u)}{\theta_u}$. In all other cases, i.e., when $m \in I_2$, there is no intersection between the beam and the first sector and the probability of achieving the maximum gain is thus zero. This proves equations (14) and (15). The same derivation also applies to the receiver side.

C. Proof of Lemma 3

The joint PMF of G_m^{T*} and G_n^{R*} is calculated considering different optimal beam pairs, which leads to (16). The joint probability $\mathbb{P}[G_m^T = \nu, G_n^R = \kappa, l^* = (m, n)]$ can be expanded into $2^{2(N_b-1)}$ terms according to the joint distribution of $\{G_i^T\}_{i \neq m}$ and $\{G_j^R\}_{j \neq n}$:

$$\begin{aligned} & \mathbb{P}[G_m^T = \nu, G_n^R = \kappa, l^* = (m, n)] \\ &= \sum_{\substack{(\nu_i, \kappa_j) \in \mathcal{G}^T \times \mathcal{G}^R \\ i \in [1:N_b] \setminus m, j \in [1:N_b] \setminus n}} \left\{ \mathbb{P}[l^* = (m, n) | G_m^T = \nu, G_n^R = \kappa, \right. \\ & \left. G_i^T = \nu_i, G_j^R = \kappa_j] \mathbb{P}[G_m^T = \nu, G_n^R = \kappa, G_i^T = \nu_i, G_j^R = \kappa_j] \right\} \quad (53) \end{aligned}$$

Since the antenna gains G_i^T and G_j^R over different beam pairs are independent, the joint distribution of $\{G_i^T\}$ and $\{G_j^R\}$ can be expressed as follows:

$$\begin{aligned} & \mathbb{P}[G_m^T = \nu, G_n^R = \kappa, \{G_i^T = \nu_i\}, \{G_j^R = \kappa_j\}] \\ &= \mathbb{P}[G_m^T = \nu] P[G_n^R = \kappa] \prod_{\substack{i \in [1:N_b] \setminus m \\ j \in [1:N_b] \setminus n}} \mathbb{P}[G_i^T = \nu_i] \mathbb{P}[G_j^R = \kappa_j] \quad (54) \end{aligned}$$

According to (11), the chosen beam pair is chosen by measuring the useful received power with different beam pairs. The conditional probability in (53) is the probability that the

received signal gets the largest power over beam pair (m, n) , which can be expressed as follows:

$$\begin{aligned} & \mathbb{P}\{l^* = (m, n) | G_n^T = \nu, G_n^R = \kappa, \{G_i^T = \nu_i\}, \{G_j^R = \kappa_j\}\} \\ &= \mathbb{E}_h \prod_{\substack{\bar{m} \in [1:N_b], \bar{n} \in [1:N_b] \\ (\bar{m}, \bar{n}) \neq (m, n) \\ \nu_{\bar{m}} = \nu, \kappa_{\bar{n}} = \kappa}} \mathbb{P}[h\nu\kappa > h(\bar{m}, \bar{n})\nu_{\bar{m}}\kappa_{\bar{n}} | h] \quad (55) \\ &= \mathbb{E}_h \prod_{\substack{\bar{m} \in [1:N_b], \bar{n} \in [1:N_b] \\ (\bar{m}, \bar{n}) \neq (m, n) \\ \nu_{\bar{m}} = \nu, \kappa_{\bar{n}} = \kappa}} F\left(\frac{h\nu\kappa}{\nu_{\bar{m}}\kappa_{\bar{n}}}\right) \quad (56) \end{aligned}$$

The CDF of the gamma distribution is expressed as $F(x) = \frac{1}{\Gamma(M)}\gamma(M, Mx)$. In order to reduce the calculation complexity, the lower incomplete gamma function $\gamma(\cdot)$ can be approximated by $\gamma(n, x) = (n-1)! \left(1 - e^{-x} \sum_{k=0}^{n-1} \frac{x^k}{k!}\right)$ [49].

D. Proof of Theorem 4

We first consider only the randomness of h_{x_o} . The conditional probability $\mathbb{P}(\mathcal{R} > \eta | \Phi^T, \Phi^R, h_x)$ is thus a constant for a given configuration (Φ^T, Φ^R) and a given value of h_x , for all $x \in \Phi^T \setminus x_o$. According to the definition of the rate in (19), we have:

$$\begin{aligned} & \mathbb{P}(\mathcal{R} > \eta | \Phi^T, \Phi^R, h_x) \\ &= \mathbb{P}\left(h_{x_o} > \left(2^{\frac{\eta}{W}} - 1\right) \frac{\sum_{x \in \Phi^T \setminus x_o} Ph_x G_x \ell(|x|) + N_0 W}{G_o P \ell(r)} \mid \Phi^T, \Phi^R, h_x\right) \\ &= 1 - \frac{1}{\Gamma(M)} \gamma\left(M, M\eta' \frac{\sum_{x \in \Phi^T} P G_x h_x \ell(|x|) + N_0 W}{P G_o}\right) \quad (57) \end{aligned}$$

$$\approx 1 - \left(1 - e^{-\beta M \eta' \frac{\sum_{x \in \Phi^T} P G_x h_x \ell(|x|) + N_0 W}{P G_o}}\right)^M \quad (58)$$

$$= \sum_{m=1}^M \binom{M}{m} (-1)^{m+1} e^{-\frac{m M \beta \eta' N_0 W}{P G_o}} \prod_{x \in \Phi^T} e^{-m \beta M \eta' \frac{G_x h_x \ell(|x|)}{G_o}} \quad (59)$$

where $\eta' = \frac{2^{\frac{\eta}{W}} - 1}{\ell(r)}$, $\gamma(\cdot)$ refers to the lower incomplete gamma function, and $\beta = [\Gamma(1+M)]^{-1/M}$. Equation (57) comes from the fact that h_{x_o} is a gamma distributed random variable. The approximation (58) is obtained by adopting the following tight inequality [50]:

$$(1 - e^{-\beta M x})^M < \frac{1}{\Gamma(M)} \gamma(M, Mx) \quad (60)$$

The conditional rate coverage can now be obtained by averaging the probability $\mathbb{P}(\mathcal{R} > \eta | \Phi^T, \Phi^R, h_{x_o})$ with respect to $h_x, x \in \Phi$. Recall that the coefficients $\{h_x\}_{x \in \Phi}$ are i.i.d. with a Gamma distribution. Thus we have the following formulas:

$$\begin{aligned} & P_c(\eta) \\ &= \sum_{m=1}^M \binom{M}{m} (-1)^{m+1} e^{-\frac{m M \beta \eta' N_0 W}{P G_o}} \prod_{x \in \Phi^T} \mathbb{E}_{h_x} \left[e^{-m \beta M \eta' \frac{G_x \ell(|x|)}{G_o} h_x} \right] \quad (61) \end{aligned}$$

$$= \sum_{m=1}^M \binom{M}{m} (-1)^{m+1} e^{-\frac{m M \beta \eta' N_0 W}{P G_o}} \prod_{x \in \Phi^T} \frac{1}{\left(1 + \frac{m \beta \eta' G_x \ell(|x|)}{G_o}\right)^M} \quad (62)$$

The b 's moment of $P_c(\eta)$ is the expectation of $P_c(\eta)^b$ with respect to Φ^T, Φ^R and the antenna gain G_o . By using the multinomial theorem [39], it can be expressed as follows:

$$\begin{aligned} M_b &= \sum_{k_1+k_2+\dots+k_M=b} \binom{b}{k_1 \dots k_M} \mathbb{E} \prod_{m=1}^M \left(\binom{M}{m} (-1)^{m+1} e^{-\frac{m M \beta \eta' N_0 W}{P G_o}} \right. \\ &\quad \left. \times \prod_{x \in \Phi^T} \frac{1}{\left(1 + \frac{m \beta \eta' G_x \ell(|x|)}{G_o}\right)^M} \right)^{k_m} \quad (63) \\ &= \sum_{k_1+k_2+\dots+k_M=b} \binom{b}{k_1 \dots k_M} \left(\prod_{m=1}^M \left(\binom{M}{m} (-1)^{m+1} \right)^{k_m} \right) \\ &\quad \times \mathbb{E}_{G_o} \left[e^{-M \beta \eta' \frac{N_0 W}{P G_o} \sum_{m=1}^M m k_m} \right. \\ &\quad \left. \times \mathbb{E}_{\Phi^T} \prod_{x \in \Phi^T} \mathbb{E}_{\Phi^R} \prod_{m=1}^M \left(1 + \frac{m \beta \eta' G_x \ell(|x|)}{G_o}\right)^{-M k_m} \right] \quad (64) \end{aligned}$$

The process Φ^R is a conditional random measure that depends both on Φ^T and the AoD of the interfering devices $\{\xi_x\}, x \in \Phi^T$, where ξ_x for different $x \in \Phi^T$ are independent. So the expectation with respect to Φ^R in (64) can be replaced by the expectation with respect to ξ_x and writes now:

$$\begin{aligned} & \mathbb{E}_{\Phi^R} \left[\prod_{x \in \Phi^T} \mathbb{E}_{\Phi^R} \left[\prod_{m=1}^M \left(1 + \frac{m \beta \eta' G_x \ell(|x|)}{G_o}\right)^{-M k_m} \right] \right] \\ &= \exp\left(-\lambda \int_{\mathbb{R}^2} 1 - \mathbb{E}_{\xi_x} \left[\prod_{m=1}^M \left(1 + \frac{m \beta \eta' G_x \ell(|x|)}{G_o}\right)^{-M k_m} \right] dx\right) \quad (65) \end{aligned}$$

The integral part in equation (65) follows from the probability generation functional (PGFL) of a Poisson point process [26]. We then denote this integral part as $Q(\eta', G_o)$ and transform it into polar form. Since ψ_x is uniformly distributed in $[0, 2\pi)$, we get:

$$\begin{aligned} & Q(\eta', G_o) \\ &= \int_{\mathbb{R}^2} 1 - \mathbb{E}_{\xi_x} \left[\prod_{m=1}^M \left(1 + \frac{m \beta \eta' G_x \ell(|x|)}{G_o}\right)^{-M k_m} \right] dx \quad (66) \\ &= \int_0^\infty \int_{-\pi}^\pi 1 \\ &\quad - \frac{1}{2\pi} \int_{-\pi}^\pi \prod_{m=1}^M \left(1 + \frac{m \beta \eta' G_x \ell(|v|)}{G_o}\right)^{-M k_m} v d\xi_x d\psi_x dv \quad (67) \\ &= \frac{1}{2\pi} \int_{-\pi}^\pi \int_{-\pi}^\pi \int_0^\infty \\ &\quad \left(1 - \prod_{m=1}^M \left(1 + \frac{m \beta \eta' G_x \ell(|v|)}{G_o}\right)^{-M k_m}\right) v dv d\xi_x d\psi_x \quad (68) \end{aligned}$$

We then let $A(\eta', G_o, G_x)$ denote the following function:

$$\begin{aligned} & A(\eta', G_o, G_x) = \\ & \int_0^\infty \left(1 - \prod_{m=1}^M \left(1 + \frac{m \beta \eta' G_x \ell(|v|)}{G_o}\right)^{-M k_m}\right) v dv \quad (69) \end{aligned}$$

Because the angles ξ_x and ψ_x are all uniformly distributed in $[0, 2\pi)$ and the antenna gain G_x is the product of $g^T(\xi_x, \theta_x^T)$

and $g^R(\psi_x, \theta_x^T)$, where θ_x^T and θ_x^R are also uniformly distributed, we get (30). Let $u = v^\alpha$ and $\delta = 2/\alpha$ we get:

$$A(\eta', G_o, G_x) = \lim_{T \rightarrow \infty} \delta/2 \int_0^T \left(1 - \prod_{m=1}^M \left(1 + \frac{m\beta\eta'G_x}{G_o u} \right)^{-Mk_m} \right) u^{\delta-1} du \quad (70)$$

By replacing u with $t = u/T$, we get:

$$A(\eta', G_o, G_x) = \lim_{T \rightarrow \infty} \frac{T^\delta \delta}{2} \int_0^1 \left(1 - \prod_{m=1}^M \left(1 + \frac{m\beta\eta'G_x}{G_o T t} \right)^{-Mk_m} \right) t^{\delta-1} dt \quad (71)$$

1) *First Moment:* In the specific case of the first moment, i.e., when $b = 1$, equation (29) can be simplified. Indeed, the sum is performed over all combinations of non negative integers k_1, \dots, k_M such that $k_1 + \dots + k_M = 1$. As a consequence, there are M such combinations, where for each combination there a single term equal to 1, say $k_m = 1$ and all others are equal to zero, i.e., $k_i = 0$ for $i \neq m$. The sum in (29) is thus now over these M combinations.

Given the derived values of the k_i , the multinomial coefficient $\binom{b}{k_1, \dots, k_M} = \frac{b!}{k_1! \dots k_M!}$ is always equal to 1. The product in (29) has a single factor: For the combination m it reduces to $\binom{M}{m} (-1)^{m+1}$. At last the expectation in (29) is reduced to $\mathbb{E}_{G_o} \left[e^{-M\beta\eta' \frac{N_0 W}{P G_o} m} e^{-\lambda Q(\eta', G_o)} \right]$ since only one term remains in the sum. We thus obtain:

$$M_1 \simeq \sum_{m=1}^M \binom{M}{m} (-1)^{m+1} \mathbb{E}_{G_o} \left[e^{-M\beta\eta' \frac{N_0 W}{P G_o} m} e^{-\lambda Q(\eta', G_o)} \right] \quad (72)$$

where Q is given by (30). Now, the function A in (31) can be also simplified using the specific expression of the k_i when $b = 1$:

$$A(m, \eta', G_o, G_x) = \lim_{T \rightarrow \infty} \frac{T^\delta \delta}{2} \int_0^1 \left(1 - \left(1 + \frac{m\beta\eta'G_x}{G_o T t} \right)^{-M} \right) t^{\delta-1} dt \quad (73)$$

$$= \lim_{T \rightarrow \infty} \frac{T^\delta \delta}{2} \int_0^1 \left(1 - \left(1 - \frac{1}{1 + \frac{G_o T t}{m\beta\eta'G_x}} \right)^M \right) t^{\delta-1} dt \quad (74)$$

By using the binomial theorem, it can be further expressed as:

$$A(m, \eta', G_o, G_x) = \lim_{T \rightarrow \infty} \frac{T^\delta \delta}{2} \sum_{n=1}^M \binom{M}{n} (-1)^{n+1} \int_0^1 \left(1 + \frac{G_o T t}{m\beta\eta'G_x} \right)^{-n} t^{\delta-1} dt \quad (75)$$

Equation (35) is derived by replacing the integral part by the integral form of the hypergeometric function ${}_2F_1$ [40]:

$$B(b, c-b) {}_2F_1(a, b; c; z) = \int_0^1 t^{b-1} (1-t)^{c-b-1} (1-tz)^{-a} dt \quad (76)$$

with $a = n$, $b = \delta$, $c = \delta + 1$ and $z = -\frac{G_o T}{m\beta\eta'G_x}$. The function $B(\cdot)$ denotes the Beta function and $B(b, c-b) = B(\delta, 1) = 1/\delta$ in our case.

Note that the expression of A and thus the expression of Q now explicitly depends on the combination m of the k_i in (72). We thus now write $Q_1(m, \eta', G_o)$ and $A_1(m, \eta', G_o, G_x)$ to distinguish these functions from their counterpart in the generic case.

2) *Second Moment:* When $b = 2$, the sum in (29) is performed over all combinations of non negative integers k_1, \dots, k_M such that $k_1 + \dots + k_M = 2$. There are thus two sub-cases: Either there is a single index equal to 2 and others equal to 0 (say $k_m = 2$ and $k_n = 0$ for $n \neq m$) or there are two indices equal to 1 and all others equal to 0 (say $k_i = k_j = 1$ and $k_n = 0$ for $n \neq i$ and j).

In the first sub-case, there are M possible combinations of the k_i and the multinomial coefficient is always equal to 1. We have thus a very similar derivation as for the first moment, except that here $k_m = 2$ instead of 1. We come up with the expression of A (renamed A_{21} to distinguish from the generic case) similar to (73):

$$A_{21}(m, \eta', G_o, G_x) = \lim_{T \rightarrow \infty} \frac{T^\delta \delta}{2} \int_0^1 \left(1 - \left(1 + \frac{m\beta\eta'G_x}{G_o T t} \right)^{-2M} \right) t^{\delta-1} dt \quad (77)$$

Equation (40) is obtained by introducing the hypergeometric function as it has been done for the first moment. The function Q_{21} is obtained by replacing A by A_{21} in (30) and showing the explicit dependence on m . For this first sub-case, we thus obtain a first term:

$$M_{21} \simeq \sum_{m=1}^M \binom{M}{m}^2 \mathbb{E}_{G_o} \left[e^{-2M\beta\eta' \frac{N_0 W}{P G_o} m} e^{-\lambda Q_{21}(m, \eta', G_o)} \right] \quad (78)$$

In the second sub-case, the sum in (29) is over all possible i and j such that $k_i = k_j = 1$, $i \neq j$. The multinomial coefficient is always equal to 2. For a given i and j , the product in (30) reduces to:

$$\binom{M}{i} \binom{M}{j} (-1)^{i+j} \quad (79)$$

and the expectation to:

$$\mathbb{E}_{G_o} \left[e^{-(i+j)M\beta\eta' \frac{N_0 W}{P G_o}} e^{-\lambda Q_{22}(i, j, \eta', G_o)} \right] \quad (80)$$

where we have renamed the function Q for this specific sub-case. At last, we come up with the expression (41) of the function A (renamed here A_{22}) similar to (73) by taking into account the specific values of the k_i . Note that the function A_{22} and hence Q_{22} explicitly depend here on the indices i and j . For the second sub-case, we thus obtain a second term:

$$M_{22} \simeq \sum_{i=1}^{M-1} \sum_{j=i+1}^M 2 \binom{M}{i} \binom{M}{j} (-1)^{i+j} \times \mathbb{E}_{G_o} \left[e^{-(i+j)M\beta\eta' \frac{N_0 W}{P G_o}} e^{-\lambda Q_{22}(i, j, \eta', G_o)} \right] \quad (81)$$

Summing M_{21} in (78) and M_{22} in (81), we obtain (37).

REFERENCES

- [1] R. I. Ansari, C. Chrysostomou, S. A. Hassan, M. Guizani, S. Mumtaz, J. Rodriguez, and J. J. Rodrigues, "5G D2D networks: Techniques, challenges, and future prospects," *IEEE Systems Journal*, vol. 12, no. 4, pp. 3970–3984, 2017.

- [2] 3GPP, "Study on physical layer enhancements for NR ultra-reliable and low latency case (URLLC)," 3rd Generation Partnership Project (3GPP), Tech. Rep. 38.824, 2019, version 16.0.
- [3] R. Liu, G. Yu, J. Yuan, and G. Y. Li, "Resource management for millimeter-wave ultra-reliable and low-latency communications," *IEEE Trans. on Communications*, vol. 69, no. 2, pp. 1094–1108, 2020.
- [4] D. Tse and P. Viswanath, *Fundamentals of wireless communication*. Cambridge university press, 2005.
- [5] S. Kuttu and D. Sen, "Beamforming for millimeter wave communications: An inclusive survey," *IEEE Communications Surveys & Tutorials*, vol. 18, no. 2, pp. 949–973, 2015.
- [6] J. Wildman, P. H. J. Nardelli, M. Latva-aho, and S. Weber, "On the joint impact of beamwidth and orientation error on throughput in directional wireless poisson networks," *IEEE Trans. on Wireless Communications*, vol. 13, no. 12, pp. 7072–7085, 2014.
- [7] M. Haenggi, *Stochastic geometry for wireless networks*. Cambridge University Press, 2012.
- [8] A. H. Sakr and E. Hossain, "Cognitive and energy harvesting-based D2D communication in cellular networks: Stochastic geometry modeling and analysis," *IEEE Trans. on Communications*, vol. 63, no. 5, pp. 1867–1880, 2015.
- [9] M. Haenggi, "The meta distribution of the SIR in poisson bipolar and cellular networks," *IEEE Trans. on Wireless Communications*, vol. 15, no. 4, pp. 2577–2589, 2015.
- [10] N. Deng and M. Haenggi, "A fine-grained analysis of millimeter-wave Device-to-Device networks," *IEEE Trans. on Communications*, vol. 65, no. 11, pp. 4940–4954, 2017.
- [11] —, "The energy and rate meta distributions in wirelessly powered D2D networks," *IEEE Journal on Selected Areas in Communications*, vol. 37, no. 2, pp. 269–282, 2018.
- [12] M. Wang, C. Zhang, X. Chen, and S. Tang, "Performance analysis of millimeter wave wireless power transfer with imperfect beam alignment," *IEEE Trans. on Vehicular Technology*, vol. 70, no. 3, pp. 2605–2618, 2021.
- [13] Y. Quan, M. Coupechoux, and J.-M. Kélif, "Rate meta-distribution in mmw D2D networks with beam misalignment," in *GLOBECOM—IEEE Global Communications Conference*. IEEE, 2022, pp. 1825–1830.
- [14] R. Wang, N. Deng, and H. Wei, "Towards a deep analysis of millimeter wave d2d underlaid cellular networks," *IEEE Transactions on Communications*, vol. 69, no. 10, pp. 6545–6560, 2021.
- [15] H. Ibrahim, H. Tabassum, and U. T. Nguyen, "The meta distributions of the sir/snr and data rate in coexisting sub-6ghz and millimeter-wave cellular networks," *IEEE Open Journal of the Communications Society*, vol. 1, pp. 1213–1229, 2020.
- [16] M. Shi, X. Gao, K. Yang, D. Niyato, and Z. Han, "Meta distribution of the sir for mmwave cellular networks with clusters," *IEEE Transactions on Communications*, vol. 69, no. 10, pp. 6956–6970, 2021.
- [17] A. Goldsmith, *Wireless communications*. Cambridge university press, 2005.
- [18] S. Hur, T. Kim, D. J. Love, J. V. Krogmeier, T. A. Thomas, and A. Ghosh, "Millimeter wave beamforming for wireless backhaul and access in small cell networks," *IEEE Trans. on communications*, vol. 61, no. 10, pp. 4391–4403, 2013.
- [19] C. Liu, M. Li, S. V. Hanly, I. B. Collings, and P. Whiting, "Millimeter wave beam alignment: Large deviations analysis and design insights," *IEEE journal on selected areas in communications*, vol. 35, no. 7, pp. 1619–1631, 2017.
- [20] Y. Li, J. G. Andrews, F. Baccelli, T. D. Novlan, and C. J. Zhang, "Design and analysis of initial access in millimeter wave cellular networks," *IEEE Trans. on Wireless Communications*, vol. 16, no. 10, pp. 6409–6425, 2017.
- [21] S. S. Kalamkar, F. Baccelli, F. M. Abinader, A. S. M. Fani, and L. G. U. Garcia, "Beam management in 5G: A stochastic geometry analysis," *IEEE Trans. on Wireless Communications*, vol. 21, no. 4, pp. 2275–2290, 2021.
- [22] A. Alkhateeb, Y.-H. Nam, M. S. Rahman, J. Zhang, and R. W. Heath, "Initial beam association in millimeter wave cellular systems: Analysis and design insights," *IEEE Trans. on Wireless Communications*, vol. 16, no. 5, pp. 2807–2821, 2017.
- [23] Y. Quan, J.-M. Kélif, and M. Coupechoux, "Spatio-temporal wireless d2d network with beamforming," in *ICC 2021 - IEEE International Conference on Communications*, 2021, pp. 1–6.
- [24] Y. Quan, M. Coupechoux, and J.-M. Kélif, "Spatio-temporal wireless d2d network with imperfect beam alignment," in *2022 IEEE Wireless Communications and Networking Conference (WCNC)*, 2022, pp. 2346–2351.
- [25] F. Baccelli and B. Błaszczyszyn, "Stochastic geometry and wireless networks: Volume i theory," *Foundations and Trends® in Networking*, vol. 3, no. 3–4, pp. 249–449, 2010.
- [26] F. Baccelli, B. Błaszczyszyn, and M. Karray, *Random measures, point processes, and stochastic geometry*. Inria, 2020. [Online]. Available: <https://hal.inria.fr/hal-02460214>
- [27] C. A. Balanis, *Antenna theory: analysis and design*. John Wiley & sons, 2015.
- [28] J. D. Kraus and R. J. Marhefka, *Antenna for all applications*. McGraw-Hill, 2002.
- [29] H. J. Visser, *Array and phased array antenna basics*. John Wiley & Sons, 2006.
- [30] M. Di Renzo, "Stochastic geometry modeling and analysis of multi-tier millimeter wave cellular networks," *IEEE Transactions on Wireless Communications*, vol. 14, no. 9, pp. 5038–5057, 2015.
- [31] Y. Xing and T. S. Rappaport, "Millimeter wave and terahertz urban microcell propagation measurements and models," *IEEE Communications Letters*, vol. 25, no. 12, pp. 3755–3759, 2021.
- [32] H. Asplund, D. Astely, P. von Butovitsch, T. Chapman, M. Frenne, F. Ghasemzadeh, M. Hagström, B. Hogan, G. Jongren, J. Karlsson *et al.*, *Advanced Antenna Systems for 5G Network Deployments: Bridging the Gap Between Theory and Practice*. Academic Press, 2020.
- [33] G. Lee, Y. Sung, and J. Seo, "Randomly-directional beamforming in millimeter-wave multiuser miso downlink," *IEEE Transactions on Wireless Communications*, vol. 15, no. 2, pp. 1086–1100, 2015.
- [34] Y. Zhou and S. Sun, "Performance analysis of opportunistic beam splitting noma in millimeter wave networks," *IEEE Transactions on Vehicular Technology*, vol. 71, no. 3, pp. 3030–3043, 2022.
- [35] 3GPP, "Nr; physical layer procedures for control." [Online]. Available: <http://www.3gpp.org/DynaReport/38213.htm>
- [36] A. Omri, M. Shafiq, A. Ali, and H. Alnuweiri, "Synchronization procedure in 5g nr systems," *IEEE Access*, vol. 7, pp. 41 286–41 295, 2019.
- [37] P. Wang and F. Berggren, "Secondary synchronization signal in 5g new radio," in *2018 IEEE International Conference on Communications (ICC)*, 2018, pp. 1–6.
- [38] Y. Polyanskiy, H. V. Poor, and S. Verdú, "Channel coding rate in the finite blocklength regime," *IEEE Transactions on Information Theory*, vol. 56, no. 5, pp. 2307–2359, 2010.
- [39] E. A. Bender and S. G. Williamson, *Foundations of combinatorics with applications*. Courier Corporation, 2013.
- [40] I. S. Gradshteyn and I. M. Ryzhik, *Table of integrals, series, and products*. Academic press, 2014.
- [41] 3GPP, "Study on New Radio (NR) access technology," 3rd Generation Partnership Project (3GPP), Tech. Rep. 38.912, 2017, version 14.0.
- [42] M. Giordani, M. Polese, A. Roy, D. Castor, and M. Zorzi, "A tutorial on beam management for 3GPP NR at mmwave frequencies," *IEEE Communications Surveys & Tutorials*, vol. 21, no. 1, pp. 173–196, 2018.
- [43] T.-K. Le, U. Salim, and F. Kaltenberger, "An overview of physical layer design for Ultra-Reliable Low-Latency Communications in 3GPP releases 15, 16, and 17," *IEEE Access*, vol. 9, pp. 433–444, 2020.
- [44] 3GPP, "Study on new radio access technology physical layer aspects," 3rd Generation Partnership Project (3GPP), Tech. Rep. 38.802, 2017, version 14.0.
- [45] V. Raghavan, S. Noimanivone, S. K. Rho, B. Farin, P. Connor, R. A. Motos, Y.-C. Ou, K. Ravid, M. A. Tassoudji, O. H. Koymen *et al.*, "Hand and body blockage measurements with form-factor user equipment at 28 ghz," *IEEE Transactions on Antennas and Propagation*, vol. 70, no. 1, pp. 607–620, 2021.
- [46] F. Fernandes, C. Rom, J. Harrebek, S. Svendsen, and C. N. Manchon, "Hand blockage impact on 5G mmwave beam management performance," *IEEE Access*, vol. 10, pp. 106 033–106 049, 2022.
- [47] B. Xue, P. Koivumaki, L. Vaha-Savo, K. Haneda, and C. Icheln, "Impacts of real hands on 5g millimeter-wave cellphone antennas: Measurements and electromagnetic models," *IEEE Transactions on Instrumentation and Measurement*, vol. 72, pp. 1–12, 2023.
- [48] A. A. Nasir, H. D. Tuan, H. H. Nguyen, M. Debbah, and H. V. Poor, "Resource allocation and beamforming design in the short blocklength regime for urllc," *IEEE Transactions on Wireless Communications*, vol. 20, no. 2, pp. 1321–1335, 2021.
- [49] H. S. Wall, *Analytic theory of continued fractions*. Courier Dover Publications, 2018.
- [50] H. Alzer, "On some inequalities for the incomplete gamma function," *Mathematics of Computation*, vol. 66, no. 218, pp. 771–778, 1997.



Yibo Quan received the B.E. degree in information engineering from the Southeast University, China, in 2017, the M.Sc. degree in advanced systems of radiocommunications from the University of Paris-Saclay, France, in 2019, and the Ph.D. degree in computer science from the Institut Polytechnique de Paris (IP Paris) in 2023. He was with the Orange Labs, France as an industrial doctoral researcher.



Marceau Coupechoux is Professor at Telecom Paris, Institut Polytechnique de Paris, France. He was a Visiting Scientist at the Indian Institute of Science, Bangalore, India, during 2011–2012. Currently, at the Computer and Network Science department of Telecom Paris, he is working on wireless networks focusing on optimization, resource allocation and environmental impact.



Jean-Marc Kelif obtained the Engineer degree in Materials and Solid State Physics Sciences from the University of Paris XIII (Villetaneuse, France) in 1984, and his Ph.D. from Telecom Paris, France. Since 1993, he has been with Orange Labs (Research Centre of Orange). His current research interests include the performance evaluation, modeling, dimensioning and optimization of wireless telecommunication networks.